Spatial Variations of the Wave, Stress and Wind Fields in the Shoaling Zone

Larry Mahrt

College of Oceanic and Atmospheric Sciences

Oregon State University

Corvallis, OR 97331

phone: (541) 737-5691 fax: (541) 737-2540 email: mahrt@oce.orst.edu

Grant #: N000149710279

http://blg.oce.orst.edu/shoaling

FINAL REPORT
17 SEPTEMBER 2001

Spatial Variations of the Wave, Stress and Wind Fields in the Shoaling Zone

Larry Mahrt

College of Oceanic and Atmospheric Sciences

Oregon State University

Corvallis, OR 97331

phone: (541) 737-5691 fax: (541) 737-2540 email: mahrt@oce.orst.edu

Grant #: N000149710279

http://blg.oce.orst.edu/shoaling

FINAL REPORT
17 SEPTEMBER 2001

Spatial Variations of the Wave, Stress and Wind Fields in the Shoaling Zone

Final Report

Larry Mahrt
College of Oceanic and Atmospheric Sciences
Oregon State University
Corvallis, OR 97331
phone: (541) 737-5691 fax: (541) 737-2540 email: mahrt@oce.orst.edu
Grant #: N000149710279
http://blg.oce.orst.edu/shoaling

LONG-TERM GOAL

Our long term goals are to improve parameterization of surface fluxes in the coastal zone in the presence of wave growth, shoaling, and internal boundary layer development. These goals include improving the present form of similarity theory used by models to predict surface fluxes and stress over water surfaces and documenting development of internal boundary layers in the coastal zone that are currently not modelled correctly, particularly in cases of flow of warm air over colder water.

OBJECTIVES

Our objectives are to provide quality controlled data sets which include spatial variation of surface fluxes, stress and wave characteristics and provide vertical structure of the wind and thermodynamic variables in the coastal zone. The objectives also include both evaluation of present formulations for surface fluxes at the air-sea interface and evaluation of model simulations of internal boundary layer development.

APPROACH

The first approach has been implementation of an extensive literature survey on existing studies of air-sea interaction in the coastal zone and internal boundary layer development. The second approach is implementation of three field programs, one completed in fall of 1997, one completed in spring of 1999 and one in fall of 1999. The spring 1999 field program was designed to study the internal boundary layer in offshore flow, particularly in stable conditions. The third approach is data analysis and evaluation of existing boundary layer and surface flux formulations. The fourth approach is model comparisons with other groups.

WORK COMPLETED

During the past year, we have concentrated on very stable conditions primarily related to flow of warm air over cold water. We have made additional progress with joint modeling studies of offshore flow with James Doyle of NRL-Monterey.

RESULTS

Analysis of LongEZ aircraft data and our SHOWEX sonic anemometer data reveal frequent occurrence of very small surface stress and roughness lengths. These very small roughness lengths with near collapse of the turbulence are generally associated with advection of warmer air from land over colder water. Numerical estimates of the

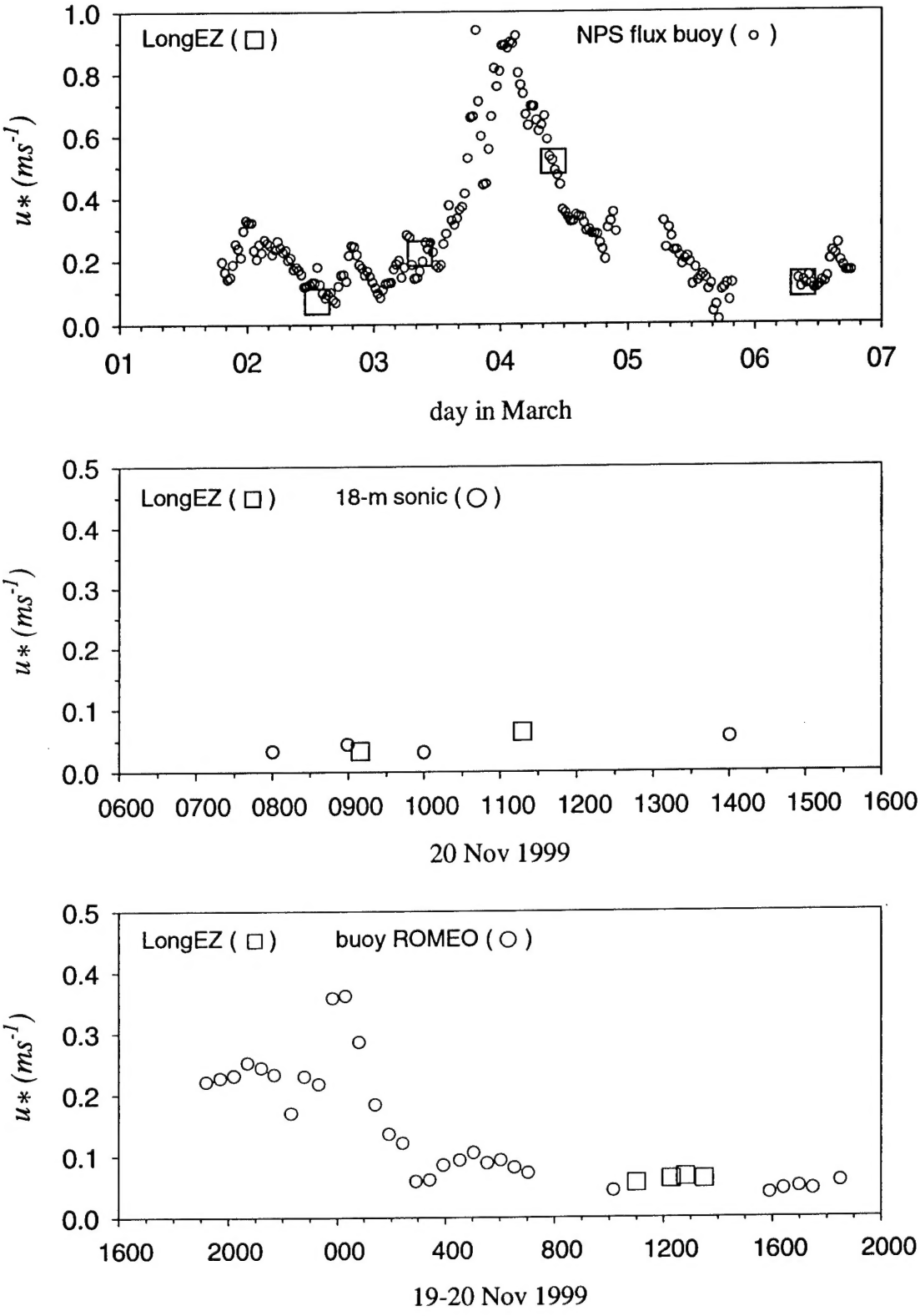

Figure 1. (a) Comparison between the friction velocity for the LongEZ and the NPS buoy

REPORT DOCUMENTATION PAGE

Form Approved
OMB No. 0704-0188

1. REPORT DATE *(DD-MM-YYYY)*	2. REPORT TYPE	3. DATES COVERED *(From - To)*
17-09-2001	Final Report	01/02/1997 - 31/21/2001

4. TITLE AND SUBTITLE

Spatial Variations of the Wave, Stress and Wind Fields in the Shoaling Zone

5a. CONTRACT NUMBER

5b. GRANT NUMBER
N000149710279

5c. PROGRAM ELEMENT NUMBER

6. AUTHOR(S)

Mahrt, Larry

5d. PROJECT NUMBER

5e. TASK NUMBER

5f. WORK UNIT NUMBER

7. PERFORMING ORGANIZATION NAME(S) AND ADDRESS(ES)

Oregon State University
312 Kerr Admin Bldg
Corvallis OR 97331-2140

8. PERFORMING ORGANIZATION REPORT NUMBER

9. SPONSORING/MONITORING AGENCY NAME(S) AND ADDRESS(ES)

Office of Naval Research
Ballston Centre Tower One
800 N Quincy St
Arlington VA 22217-5660

10. SPONSOR/MONITOR'S ACRONYM(S)

11. SPONSORING/MONITORING AGENCY REPORT NUMBER

12. DISTRIBUTION AVAILABILITY STATEMENT

Approved for Public Release; Distribution is Unlimited

13. SUPPLEMENTARY NOTES

14. ABSTRACT

We have used fast response atmospheric measurements from a small low-flying research aircraft, a tower at the end of a pier and offshore buoys to study air-sea interaction in the coastal zone. The research aircraft also measures the wave field using three downward pointing lasers. Our analysis of this data indicates that the influence of shoaling waves is significant but less important than originally thought. Nonetheless, computer models of air-sea interaction fail to properly account for the important influence of the surface wave state. Atmospheric flow of warm air over a colder sea surface can lead to complete collapse of the atmospheric turbulence and sea state. This collapse is not presently simulated in boundary layer models.

15. SUBJECT TERMS

wave stress, shoaling, coastal zone, bulk aerodynamic

16. SECURITY CLASSIFICATION OF:			17. LIMITATION OF ABSTRACT	18. NUMBER OF PAGES	19a. NAME OF RESPONSIBLE PERSON
a. REPORT	b. ABSTRACT	c. THIS PAGE			Larry Mahrt
					19b. TELEPONE NUMBER *(Include area code)* (541)737-5691

for the period of overlapping observations in March 1999, b) comparison between the LongEZ friction velocity and that for the 18-m sonic anemometer on 20 November 1999 and c) comparison between the LongEZ friction velocity and that for buoy Romeo on 20 November 1999.

aerodynamic roughness length may be subject to large errors for weak surface fluxes in very thin boundary layers because of significant random flux errors, systematic small scale flux loss, errors due to fluctuations of the aircraft altitude and errors in the estimated mean wind speed by the aircraft. With very thin stable boundary layers, the stress may decrease significantly between the surface and the observational level. In this case, Monin-Obukhov similarity theory does not apply at the observation level and the roughness length computed from the data must compensate for this inapplicability. In spite of the above observational difficulties, the small values of the momentum flux inferred from the aircraft data also occur with sonic anemometer data collected from buoys and a tower at the end of a 570-m pier (Figure 1). Ultra-smooth values of the aerodynamic roughness length do not necessarily imply specific information on the wave state. The value of the aerodynamic roughness length only provides the correct flux at the observational height, given the specified stability functions, and its relationship to wave state in these cases is uncertain.

The influence of warm air advection extends the influence of land off the coast for tens of kilometers or more. The very small roughness lengths for stable conditions are partly due to reduction of the downward momentum flux by the stable stratification. The data also show the usual minimum of the roughness length and neutral drag coefficient for wind speeds of about 5 m/s. The larger values of the roughness length at weaker wind speeds are partly associated with large deviations of the stress direction from opposite to the wind vector, apparently due to the influence of swell. The very small roughness lengths are most likely to occur with a combination of intermediate wind speeds and stable stratification. Significant wind speed is required here to maintain the advection of warmer air over the cooler sea.

In some stable cases, the vertical transport of turbulence may be downward, implying that the main source of turbulence is above the surface-based stable layer. In these cases, the aerodynamic roughness length is much larger than that for the usual case of upward transport of turbulence energy. The multitude of physical influences on the surface stress and the difficulty of measuring weak momentum fluxes prevent categorical conclusions.

The joint modeling work with James Doyle and also "in-house" work indicates that existing mesoscale/regional models can simulate some aspects of offshore flow. Errors are largest for stable conditions associated with advection of warmer air over colder water. The model can simulate the formation of the very thin stable marine layer only with extremely fine vertical resolution, on the order of one meter. However the TKE models have not been able to simulate the shear-generation of turbulence at the top of the marine layer and downward transport of turbulence toward the sea surface. The restrictive format of the mixing length parameterization seems to be the primary source of the difficulties.

IMPACT/APPLICATION

Existing concepts of marine boundary layers and air-sea interaction are inadequate in very stable conditions associated with warm air advection over colder water. Existing boundary-layer models cannot simulate this case.

RELATED PROJECTS

Analysis of offshore tower eddy correlation data from two Scandanavian sites is being carried out under grant N00014-98-0282 from the Office of Naval Research. This data allows analysis of detailed vertical structure in the lowest 40 m whereas the above work concentrates on horizontal structure in the coastal zone.

PUBLICATIONS

Vickers, D., L. Mahrt, J. Sun and T. Crawford, 2001: Structure of offshore flow. *Monthly Weather Review*, **129**, 1251-1258.

Sun, J., D. Vandemark, L. Mahrt, D. Vickers, T. Crawford and C. Vogel, 2001: Momentum transfer over the coastal zone. To appear in *J. Geophys. Res.*

Mahrt, L., D. Vickers, J. Sun, T. Crawford, G. Crescenti, and P. Frederickson, 2001: Surface stress in offshore flow and quasi-frictional decoupling. To appear in *J. Geophys. Res.*

Surface stress in offshore flow and quasi-frictional decoupling

L. Mahrt,[1] Dean Vickers,[1] Jielun Sun,[2] Timothy L. Crawford,[3]
Gennaro Crescenti,[3] and Paul Frederickson[4]

Abstract. Aircraft data collected at approximately 15 m above the sea surface in the coastal zone are analyzed to examine the spatial distribution of surface stress. Advection of stronger turbulence from land dominates the near-surface turbulence for the first few kilometers offshore. With offshore flow of warm air over cold water, strong stratification leads to very small surface stress. Because the stability restricts the momentum transfer to the waves, the aerodynamic surface roughness decreases to very small values, which in turn decreases atmospheric mixing. The redevelopment of the boundary layer farther downstream is examined. Computation of fluxes from observations for stable cases is difficult due to a variety of errors including large random flux errors, possible instrumental loss of small-scale flux, difference between the surface flux and that at the observational level, and inadvertent capture of mesoscale motions in the computed turbulent fluctuations. Although the errors appear to be substantial, the aircraft momentum fluxes compare favorably with those from sonic anemometers on two buoys and a tower at the end of a 570-m pier, even with near collapse of the turbulence.

1. Introduction

Existing models of the air-sea interaction sometimes break down in the near-coastal zone due to advection of stronger turbulence and temperature from land, nonstationarity associated with diurnally varying horizontal pressure gradients in the atmosphere, complex wave states, including young wind-driven waves and incoming swell, and shoaling of such swell. A number of studies have formulated transfer coefficients in terms of fetch [*Perrie and Toulany*, 1990] or wave age [e.g., *Geernaert et al.*, 1987; *Toba and Koga*, 1986; *Maat et al.*, 1991; *Vickers and Mahrt*, 1997a].

Advection of stronger turbulence from land can strongly influence the air-sea interaction in offshore flow [*Mahrt et al.*, 2001; *Vickers et al.*, 2001]. Some of the perceived dependence on wave age in offshore flow, whether based on friction velocity or wind speed, may be due to the influence of advection of stronger turbulence from the land surface, which decays in the downstream direction and influences the drag coefficient in a manner similar to the wave age dependence [*Sun et al.*, 2001]. This advection links the fluxes over the sea with the characteristics of the upstream land surface. *Winstead and Young* [2000] and N. Winstead and P. Mourad (Shallow great lakes scale atmospheric thermal circulation imaged by synthetic aperture radar; submitted to *Monthly Weather Review*, 2001) find that alongshore variation of land characteristics (farmland, woods, and towns) leads to alongshore variation of high-frequency surface wave energy in offshore flow; more wave energy is generated downstream from rougher land surfaces.

With offshore flow of warm air over cool water, the turbulence and surface stress can become suppressed by the stratification, referred to as quasi-frictional decoupling by *Smedman et al.* [1997a, 1997b], perhaps analogous to development of the very stable nocturnal boundary layer over land. Over land, surface cooling and stratification of the air near the surface reduces turbulence and downward heat flux, which leads to stronger net cooling of the surface and further enhancement of the stratification. Over the water the surface temperature is more constant, but the reduction of downward momentum flux by the stratification reduces generation of the surface wave field, which in turn reduces the surface roughness [*Plant et al.*, 1998] and subsequently reduces mechanical generation of atmospheric turbulence. Over land the roughness length is normally considered to be a constant for a given location and wind direction.

The partial collapse of turbulence in offshore flow of warm air over cooler water is emphasized in this study because it is the case most poorly simulated by existing models. On the basis of observations in the coastal zone in the Baltic Sea, *Smedman et al.* [1997b] find that the atmospheric boundary layer over the Baltic Sea is stable more often than unstable and the influence of warm air advection from land can extend 150 km offshore. In this study, offshore flow will be examined in terms of eddy correlation aircraft data collected approximately 15 m above the sea surface (section 3). In the next section we review the basic formulations required for the analysis in sections 4–7, using the data described in section 3.

2. Existing Parameterization of the Surface Stress

The drag coefficient is computed as

$$C_d = \frac{u_*^2}{\overline{U}^2}, \tag{1}$$

where u_* is the friction velocity based on averaged components of the stress vector and U is the wind speed computed from

[1]College of Oceanic and Atmospheric Sciences, Oregon State University, Corvallis, Oregon, USA.
[2]National Center for Atmospheric Research, Boulder, Colorado, USA.
[3]NOAA Air Resources Laboratory, Idaho Falls, Idaho, USA.
[4]Naval Postgraduate School, Monterey, California, USA.

Paper number 2000JD000159.
0148-0227/01/2000JD000159$09.00

averaged wind components. Given observations of the wind speed and surface stress, the roughness length can be "backed out" of the similarity prediction of the drag coefficient.

$$C_d = \left[\frac{\kappa}{\ln (z/z_o) - \psi_m} \right]^2, \quad (2)$$

where z is the observational level, z_o is the roughness length for momentum, κ is the von Karmen constant, taken as 0.4, and ψ_m is a function of the stability z/L, where L is the Obukhov length, expressed as

$$L = - \frac{u_*^3}{(\kappa g/\theta_v)([w'\theta'] + 0.61\theta[w'q'])}, \quad (3)$$

where θ is the potential temperature and q is the specific humidity. The stability function will be computed from *Paulson* [1970] for unstable conditions and from *Dyer* [1974] for stable conditions.

Using (2), the aerodynamic roughness length z_o can then be estimated from the observed values of u_*, U, and L and the specified function ψ. The computed roughness lengths could include compensation for incorrect stability functions ψ. However, Monin-Obukhov similarity theory was found to be a good approximation for the flux-gradient relationship in quasi-stationary homogeneous flow over the sea in terms of the turbulence energy budget [*Edson and Fairall*, 1998; *Wilczak et al.*, 1999] and flux-gradient relationship [*Vickers and Mahrt*, 1999], although modest adjustments of the stability function were suggested in the later study. The dependence of the roughness length on stability is equivalent to a dependence of the neutral drag coefficient on stability. Often the drag coefficient is reduced to a neutral value to remove the influence of stability. The neutral drag coefficient may exhibit a dependence on stability, which is sometimes interpreted as failure of Monin-Obukhov similarity theory or a failure of the existing stability functions. However, the reduction of the drag coefficient to neutral conditions assumes either constant roughness length or the Charnock formulation [*Charnock*, 1955] with constant coefficient. Both assumptions may be incorrect and are not a part of Monin-Obukhov similarity theory. Therefore a stability-dependent roughness length is not necessarily an indicator of the failure of Monin-Obukhov similarity theory.

3. Data and Analysis

Surface fluxes are estimated for the Shoaling Waves Experiment (SHOWEX) in October–November 1997 and March 1999 and in November–December 1999 [*Sun et al.*, 2001; *Crescenti et al.*, 1999; *French et al.*, 2000] using the low-level aircraft data from 37 flights on 35 days at an average height 15 m above the sea surface. The data were collected by the LongEZ research aircraft over Atlantic coastal water off the Outer Banks near Duck, North Carolina. The SHOWEX data have minimal instrumentation problems compared with the previous two field programs and several improvements in preprocessing and will be emphasized in this study.

For both experiments in 1999, a Campbell CSAT sonic anemometer (10-cm path length) operated at approximately 18 m above the water on a tower at the end of a 570-m pier (U.S. Army Corps of Engineers Field Research Facility). In November–December 1999 a second CSAT sonic anemometer was deployed on a 3-m boom attached to the top of the railing at the end of the pier, 8 m above the sea surface. To avoid serious flow distortion, we include only those time periods with winds from the northerly sector between 295 and 70 degrees for the northward pointing sonic anemometer on the rail, and easterly flow between 360 and 180 degrees for the eastward pointing 18-m sonic on the tower. Smoke releases indicated that the distortion due to the pier for the accepted wind directions did not extend to the end of the 3-m boom, which is consistent with the close agreement between the fluxes computed from the 18- and 8-m sonic anemometers. Both the aircraft and sonic anemometer data were subjected to quality control procedures similar to those described by *Vickers and Mahrt* [1997b].

3.1. Flight Pattern and Analysis Strategy

Thirteen flights from the three experiments measured horizontal and vertical structure in the lowest few hundred meters above the sea surface in the first 10–20 km offshore. Other types of flight patterns include a series of flight tracks parallel to the shore, box patterns, 100-km transects perpendicular to the coast, and a few mission-specific patterns. For the analyses in sections 4–7, all flights are used that collected low-level data over the Atlantic side of the Outer Banks with a fetch greater than 10 km for offshore flow.

3.2. Vertical Flux Divergence

Smedman et al. [1997a, 1997b] point out that the boundary layer may be very thin in stable conditions over the sea and that standard observational levels may be too high to estimate surface fluxes. Even though the LongEZ generally flew about 15 m above the sea surface, the difference between the flux at this level and the sea surface stress may be significant in thin boundary layers or advective conditions. The difference between the stress at the aircraft level and the sea surface is constrained by the equation of motion. Integrating the equation of motion for the offshore flow component between the surface and the aircraft level, z, for stationary flow, the surface stress is

$$\overline{w'u'}_{sfc} = \overline{w'u'}_z - \int_{sfc}^{z} \left[\bar{u} \frac{\partial \bar{u}}{\partial x} + \bar{w} \frac{\partial \bar{u}}{\partial z} + \frac{\partial \overline{u'^2}}{\partial x} \right] dz + \int_{sfc}^{z} f(\bar{v} - V_G)\, dz, \quad (4)$$

where we have neglected derivatives parallel to the coast (here the y direction), f is the Coriolis parameter, and V_G is the geostrophic wind. The difference between the momentum flux at the sea surface and at the observational level $z \approx 15$ m is constrained by the magnitude of the advection, horizontal flux divergence, and the ageostrophic term (the last term on the right-hand side).

Vickers et al. [2001] find that within the first few kilometers downstream from the coast, strong horizontal advection of weaker momentum is partially balanced by vertical convergence of the downward turbulent momentum flux and downward advection of stronger momentum by mean subsidence. The subsidence is associated with acceleration of offshore flow. On the basis of x-z cross-section analysis of the stress in stable offshore flow using multiple aircraft levels, *Vickers et al.* [2001] found the surface stress to be typically of the order of 10^{-2} m^2 s^{-2} smaller than the stress at the 15-m aircraft level in the first few kilometers of offshore flow. This difference can be more than 30% of the absolute flux value.

Farther offshore, advection terms become small but the depth of the turbulence might be very thin (section 6). Then

the stress divergence between the aircraft level and the surface is supported by the large-scale ageostrophic flow $f(\bar{v} - V_G)$, which is expected to be of the order of 10^{-4} m s^{-2}. This value corresponds to a change of stress of 1.5×10^{-3} m^2 s^{-2} between the surface and the aircraft level. This value is only a little smaller than the smallest stress values observed in stable offshore flow (section 4) and therefore could be important. That is, the stress at 15 m might be significantly smaller than that at the sea surface.

The influence of the height of the platform on the computed roughness length will be an important concern in this study. The height of the aircraft for low-level flights included here ranged from roughly 10 m to a specified upper cutoff of 20 m. Roughness lengths computed from the aircraft data within this range of heights do not show a clear dependence on the height of the aircraft. Comparison of the two levels of momentum and heat flux measurements at the end of the pier for onshore flow shows good agreement. However, the computed roughness length is systematically smaller at the 18-m level. This appears to be due to the increase of wind speed with height faster than predicted by similarity theory. Perhaps the 18-m level is often above the surface layer, which would also imply that the aircraft was sometimes above the surface layer.

3.3. Variable Averaging Length

In this study the dependence of the fluxes on averaging scale is studied in terms of multiresolution cospectra [e.g., *Howell and Mahrt*, 1997], which can be thought of as a wavelet decomposition using unweighted averaging lengths of different (dyadic) lengths as the local basis set. Interpretation of such cospectra does not require the assumption of periodicity, and the properly integrated multiresolution cospectra exactly satisfy Reynolds averaging.

For very stable conditions, fluxes can be quite small and confined to small horizontal scales, less than 100 m. As a result, the usual use of a 1-km window may capture significant nonturbulent mesoscale flux, which can be primarily flux sampling errors. Normally, this mesoscale flux is small compared with the turbulent flux. However, with very stable conditions, the turbulent flux is small, and the mesoscale scale flux may even dominate the computed flux. Therefore we have used a smaller averaging window to define perturbations for very stable conditions. The averaging length is determined separately for each 5-km record based on an empirical relationship (constructed below) between the averaging length and the bulk Richardson number,

$$Rb = \frac{g}{\theta}\frac{\delta\theta z}{U^2}, \qquad (5)$$

where $\delta\theta$ is the difference of potential temperature between the aircraft level and the sea surface. The bulk Richardson number is used instead of z/L, since the later is a stronger function of the averaging length itself. The sea surface temperature measured from the LongEZ was calibrated using buoy measurements for each flight day.

The length scale associated with the gap region separating turbulence and mesoscale transport is estimated from cospectra of momentum, heat, and moisture for individual flights (Figure 1). A gap scale was identified when the slope of the cospectra changed sign or when the cospectra crossed zero for length scales exceeding an arbitrary threshold of 100 m. For most flights the gap scales identified for each of the three

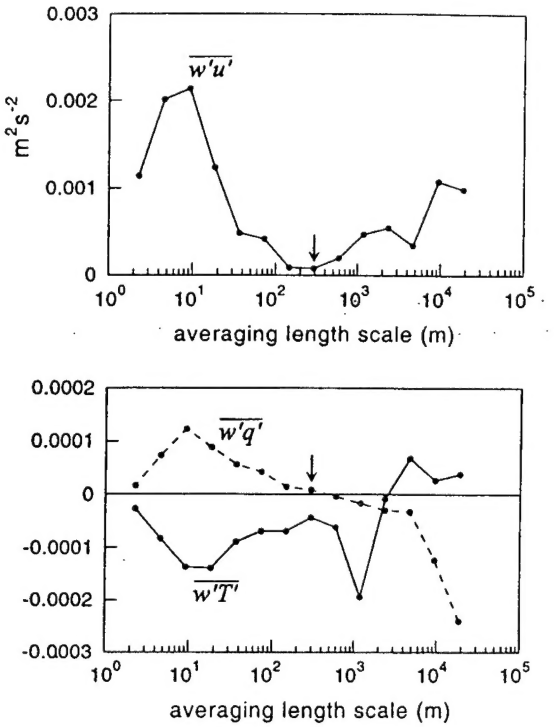

Figure 1. Determination of the averaging length based on the cospectral gap or cospectral sign reversal (vertical arrow) for (a) momentum flux (m^2 s^{-2}), and (b) heat flux (m s^{-1} °C) (solid line) and moisture flux (m s^{-1} g kg^{-1}) (dashed line) in stable conditions for a single aircraft pass on November 21.

cospectra were approximately equal. When the gap scales for the momentum, heat, and moisture fluxes were not the same, we chose an average value even though the gap scale often seemed better defined for moisture where the cospectra typically changed sign in the gap region (cospectral zero crossing).

The values of the gap scale, averaged for different intervals of Rb (Figure 2), were fit to a simple model where horizontal length scale decreases from near 5 km for unstable conditions to only 100 m for very stable conditions (Figure 2). The fluxes based on deviations from the stability-dependent averaging

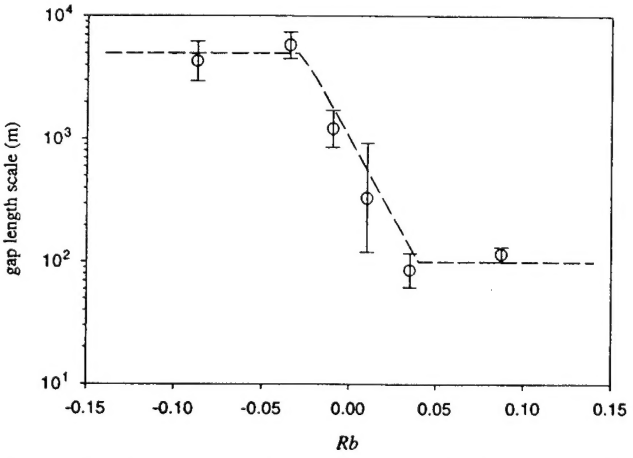

Figure 2. Dependence of the flux averaging length on the bulk Richardson number for bin-averaged values (circles) with the standard error indicated by vertical brackets, and the simplified model fit (dashed line).

length are then averaged over 5-km segments to reduce random flux errors. Application of the variable averaging length tends to increase the fluxes in unstable conditions, on average, and decrease fluxes in stable conditions, on average. However, this systematic change is small, and application of the variable averaging length does not influence the qualitative conclusions of sections 4–7. The most significant change is a reduction of heat flux for stable conditions; however, this changes the log of the roughness length by less than 10%, on average.

3.4. Other Flux Computation Problems

The aircraft data were collected at 50 samples s^{-1} with an air speed of about 55 m s^{-1}, corresponding to a sample interval of about 1 m. Fluxes on horizontal scales smaller than 2 m are lost. This small-scale flux is expected to be missing since the data were low-pass filtered to remove noise at smaller scales. As a result, there is no folding back of small-scale flux to lower frequencies via aliasing. In semicollapsed situations the cospectra do not decrease to small values at the smallest resolvable scale of about 2 m. This implies that momentum flux occurs at even smaller scales. In fact, in a few cases, the cospectra appeared to peak at scales less than 10 m!

As a measure of potential flux loss, we examined the ratio of the flux at the smallest dyadic scale of the multiresolution cospectra to the total flux. With no small-scale flux loss, this ratio should be small. For the momentum flux this ratio increases with stability as the transporting eddies shift to smaller scales, averaging 10% for very stable conditions.

In addition, significant heat flux may be lost for very stable conditions due to the response time of the thermistor, which corresponds to a horizontal scale of 3–4 m. The cospectra of the heat flux tends to vanish at the smallest resolvable scale because the sensor could not resolve variations on this scale. Greater heat flux loss compared with the momentum flux loss causes the estimated stability z/L to be too small. For stable conditions this error acts to underestimate the stability function and therefore to underestimate the roughness length computed from (2). In subsequent sections we use fluxes where no attempt was made to correct for small-scale flux loss, which is under further investigation.

Fluctuations of the aircraft height above the surface, typically of the order of a few meters on a horizontal scale of a kilometer, lead to artificial fluctuations in the presence of mean vertical gradients. The corresponding error for the momentum flux is normally small for unstable conditions. It is large for individual stable records but is not systematic (it occurs with either sign with equal probability) except for very stable conditions, where it acts to overestimate the momentum flux, on average, by 40–50%. The corresponding error in the heat flux is very small. The net effect is to underestimate z/L and the aerodynamic roughness length. Analysis of such errors is complicated and will be reported on in a future paper. Finally, the aircraft may overestimate the wind speed in weak wind conditions, causing the drag coefficient and roughness length to be underestimated.

While the above flux uncertainties seem complex and serious, the aircraft fluxes did compare well with one week of fluxes acquired by the Naval Postgraduate School flux buoy located 10.5 km off the coast (Duck) in 23 m of water (see Figure 5, section 5.1). The LongEZ flew four flights over the buoy during the first week of March 1999. The fluxes from the LongEZ and buoy agreed within the random flux error. On March 2 and 4 the surface friction velocity was small, approximately 0.1 m s^{-1} for both platforms. Stress values from the aircraft data also agree reasonably well with measurements from sonic anemometers mounted on buoys and a sonic anemometer on an offshore tower during SHOWEX (section 5.1). Agreement between instruments does not necessarily imply accurate fluxes since all of the above platforms may underestimate the flux in stable conditions.

Computation of the roughness lengths using Monin-Obukhov similarity theory may be inapplicable if the stress does not approximately oppose the wind. The stress direction may be altered by swell. The influence of swell for weak wind conditions [*Smedman et al.*, 1999; *Grachev and Fairall*, 2001] can cause upward momentum flux from the wave field to the atmosphere, in which case the aerodynamic roughness length has no meaning. In the subsequent analyses we eliminate data where the stress direction deviated by more than 45 degrees from the vector opposite the wind direction. This condition leads to a reduction of the averaged roughness length for weak wind speeds (section 7).

4. Near-Coastal Zone

To organize the discussion, we define three offshore zones for the flow of warm air over cold water: The first is the near-coastal zone, where the stress and roughness length decrease rapidly with fetch in the first few kilometers offshore for stable conditions (Figure 3, solid lines); the second is the quasi-frictional decoupling zone (section 5), where the stress and roughness length maintain extremely small values, often for more than 20 km offshore; the third is the recovery zone, where the stress and roughness length increase, sometimes abruptly (section 6).

Vickers et al. [2001] found that in the first few kilometers offshore, vertical convergence of the downward momentum flux acts to accelerate the flow in the downstream direction. At a fixed point the flow is relatively stationary. The vertical transport of turbulence energy for short fetch is also downward (Figure 4). This downward transport contrasts with the normal concept of a boundary layer, where the vertical transport of turbulence energy is either upward or small. Here this downward transport of turbulence is expressed in terms of the vertical velocity variance since the horizontal velocity variances are more sensitive to choice of averaging length. The vertical transport of the vertical velocity variance ($\overline{w'^3}$) is upward for all of the unstable cases and significantly downward for four of the seven stable cases.

Downstream from the coast the roughness length is expected to increase with wave age (C_p/u_*) with very young wind-driven waves due to increasing amplitude of the waves, until a wave age of 5–10 [e.g., *Nordeng*, 1991], where C_p is the phase speed of the dominant wave. As the wave age increases further, the roughness length decreases due to increasing phase speed of the wind-driven waves and reduction of the relative flow over the waves. The initial stage of increasing stress with increasing fetch, due to wave initiation, is not observed in our data because of the greater influence of advection of turbulence from land [*Sun et al.*, 2001]. Beyond this conclusion, effects of wave state and advection of stronger turbulence from land are difficult to isolate. The advection of stronger turbulence from land can lead to greater downward transport of momentum over the sea, which presumably enhances wave growth, just downstream from the coast.

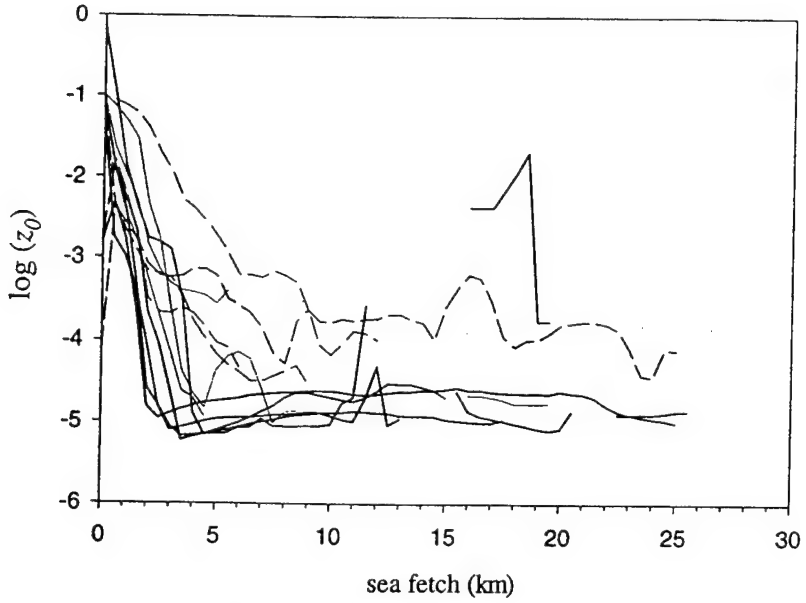

Figure 3. The roughness length as a function of fetch based on heat and momentum fluxes extracted from the 10-m level of the cross-section analyses (section 3.1) for unstable (broken lines) and stable (solid lines) conditions. To remove some extremely small values of roughness lengths and restrict the vertical range of the plot, the roughness length is not allowed to decrease below the smooth flow value (for this plot only). This condition accounts for leveling off of the roughness length in stable cases beyond a fetch of a few kilometers.

5. Quasi-frictional Decoupling Zone

In flow of warm air over cooler water, the stress, turbulence energy, and roughness length decrease by orders of magnitude in the first few kilometers offshore (Figure 3), as opposed to near-neutral and unstable conditions, where they decrease much more slowly. Therefore the stability over the water affects the rate of decrease of the turbulence downstream from the coast. The reduction of downward momentum transfer by the atmospheric stability restricts wave generation and causes very small surface roughness lengths (Figure 3), as previously noted by *Plant et al.* [1998]. These very small surface roughness lengths, in turn, lead to weaker turbulent mixing, and so forth. With such decoupling "quasi-frictional decoupling" [*Smedman et al.*, 1997b], the observed aerodynamic roughness length decreases to values several orders of magnitude smaller than the smooth flow value, as also found here. In this study we will loosely refer to quasi-frictional decoupling as cases where the computed roughness length becomes comparable to or substantially less than the smooth flow value. While we recognize that the roughness length may be significantly underestimated (section 3), these conditions correspond to very weak turbulence and values of the friction velocity significantly less than

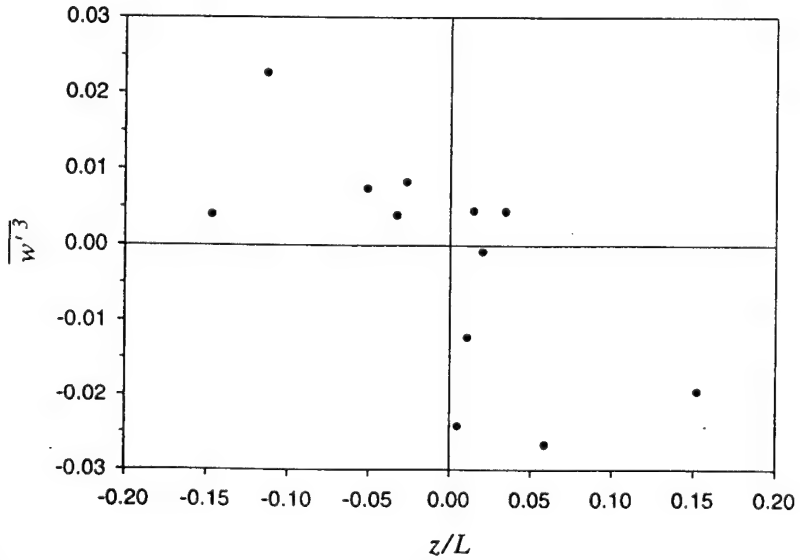

Figure 4. The vertical transport of vertical velocity variance, averaged over the first 2 km offshore as a function of stability.

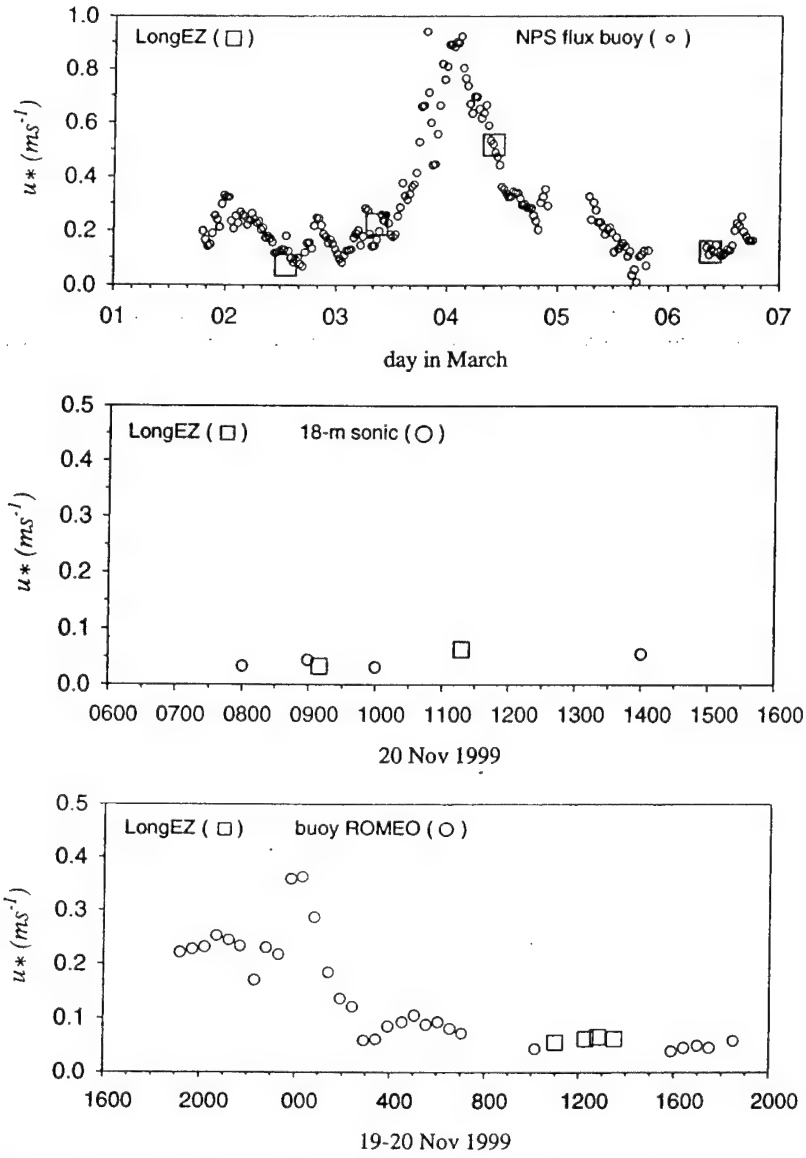

Figure 5. (a) Comparison between the friction velocity for the LongEZ and the Naval Postgraduate School buoy for the period of overlapping observations in March 1999, (b) comparison between the LongEZ friction velocity and that for the 18-m sonic anemometer on November 20, 1999, and (c) comparison between the LongEZ friction velocity and that for buoy Romeo on November 20, 1999.

0.1 m s^{-1}. These small values imply that the flow at the observational level is not fully coupled to the surface in the sense of the usual atmospheric boundary layer.

Here the quasi-frictional decoupling at the observational level begins with travel times typically of the order of 10 min, generally corresponding to fetches greater than 3–5 km (Figure 3), depending on wind speed and upstream turbulence over the land. Even though z/L is significant positive, the buoyancy flux can be relatively small because u_* is small.

5.1. Ultrasmooth

Donelan [1990, p. 265] also calls attention to extremely small roughness lengths referred to as "ultrasmooth" conditions. Variations of surface tension and only small differences between the dominant wave phase speed and wind speed were cited as possible causes. The latter does not appear to be the cause near the coast in this study, where the wind-driven waves are young and the swell opposes the offshore flow. It must be remembered that the aerodynamic roughness length is computed using the stability functions (section 2) and as such does not necessarily have a definable relation to wave state. In other terms, ultrasmooth values of the aerodynamic roughness length do not necessarily imply glassy seas.

While observational errors are large for cases of weak fluxes (section 3), sonic anemometer data show a similar semicollapse of the turbulence. Sonic anemometer measurements at the end of the 570-m pier can be used only with onshore flow where the influence of flow distortion from the tower and the pier is minimized. On November 20, 1999, the flow was weak onshore, with a stable air-sea temperature differences of about 1°C. On this day the friction velocity from the tower (Figure 5b), the buoy Romeo (Figure 5c) (provided by W. Drennen), and the aircraft all show small friction velocity values of approximately 0.05 m s^{-1}. Good agreement is also shown be-

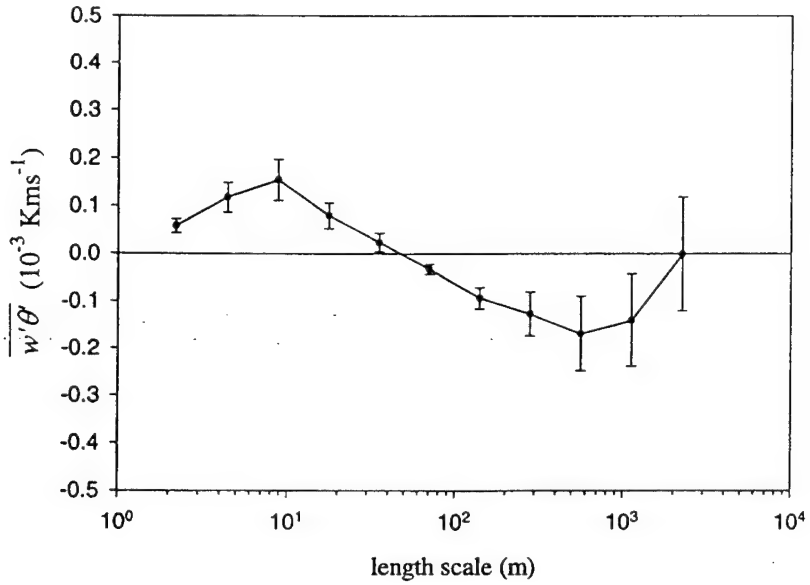

Figure 6. Kinematic heat flux as a function of horizontal scale composited for the seven passes for November 20, 1999. The vertical brackets indicate the standard error based on the between-pass variability for the seven passes.

tween the LongEZ friction velocity and that from the Naval Postgraduate School buoy [*Frederickson and Davidson*, 2000] for the overlap period in March of 1999 (Figure 5a), including a semicollapsed period. We conclude that the surface stress is extremely small but cannot categorically conclude ultrasmooth conditions because of potentially significant flux errors.

The cospectra on this day systematically show upward heat flux at horizontal scales smaller than 50 m and downward heat flux at larger scales (Figure 6). Apparently, the initial overturning corresponds to downward heat flux which destabilizes the flow (cold air on top of warm air). This destabilization leads to upward heat flux by smaller-scale eddies. *Piccirillo and Van Atta* [1997] also find upward buoyancy flux on smaller scales and downward buoyancy flux on larger scales in a stratified wind tunnel with shear. This small-scale upward heat flux was not a systematic condition for stable conditions in SHOWEX.

5.2. Minimum Wind Speed

With offshore flow of air several degrees warmer than the sea surface temperature, ultrasmooth roughness lengths are computed from the present data even for 15-m wind speeds exceeding 10 m s^{-1}. For example, on March 18, 1999, the wind speed reached 12 m s^{-1} while the friction velocity and standard deviation of the vertical velocity both fell below 0.1 m s^{-1}, corresponding to values of the roughness length smaller than the smooth flow value.

This finding for very stable conditions contrasts with the literature where the minimum wind speed for generation of surface waves is considered to be much smaller. The smooth flow regime is often thought to occur, on average, when the wind speed is less than 2.8 m s^{-1} [*Kitaigorodski and Donelan*, 1984] although smooth flow viscous effects can be important up to wind speeds of about 7.5 m s^{-1}. *Kahma and Donelan* [1987] report a range of minimum wind speeds between 0.4 and 5.5 m s^{-1} for initiation of capillary-gravity waves in a laboratory environment. On the basis of radar backscatter, the minimum wind speed for generation of surface waves is estimated to be in the range from 1.0 to 2.0 m s^{-1} [*Moller et al.*, 2000; *Plant et al.*, 1999], although a variety of observational errors for weak wind conditions have been noted [*Moller et al.*, 2000; *Freilich and Dunbar*, 1999; *Weissmann and Graber*, 1999].

6. Recovery Zone

Theoretically, one might expect slow recovery from quasi-frictional decoupling, induced by gradual development of the wave field responding to the weak surface stress, and gradual reduction of the stratification near the surface as the air-sea temperature difference decreases downstream. However, in practice, spatial variation of the sea surface temperature and wind field seem to be more important on a given day, and the recovery from quasi-frictional decoupling seems to assume a different form for each available case. The recovery can take the form of a sudden redevelopment of turbulence, and the turbulence may collapse again farther downwind. However, for most of the cases, the turbulence did not recover within the observational domain, typically extending to 10–20 km from the coast.

For example, the roughness length is still at the smooth flow value, or smaller, at 20-km fetch for four of the five cases of offshore stable flow with complete data coverage out to 20 km (Figure 3). The fifth case, on March 6, 1999, indicates rapid enhancement of the roughness length at 15–20 km offshore. This recovery to large roughness lengths is characterized by downward transport of turbulence energy from higher levels. The latter suggests that the turbulence originates from instability above the thin, cool marine layer and then is transported downward toward the surface. Perhaps the generation of this turbulence is associated with the acceleration of the decoupled flow and enhanced shear above the thin, cool marine layer.

Only limited information is available on the vertical structure in the recovery zone. On November 3, 1997, the flight plan was devoted to sampling the vertical structure of the boundary layer through numerous slant soundings from the coast out to 100 km. On this day the flow was offshore and slightly warmer

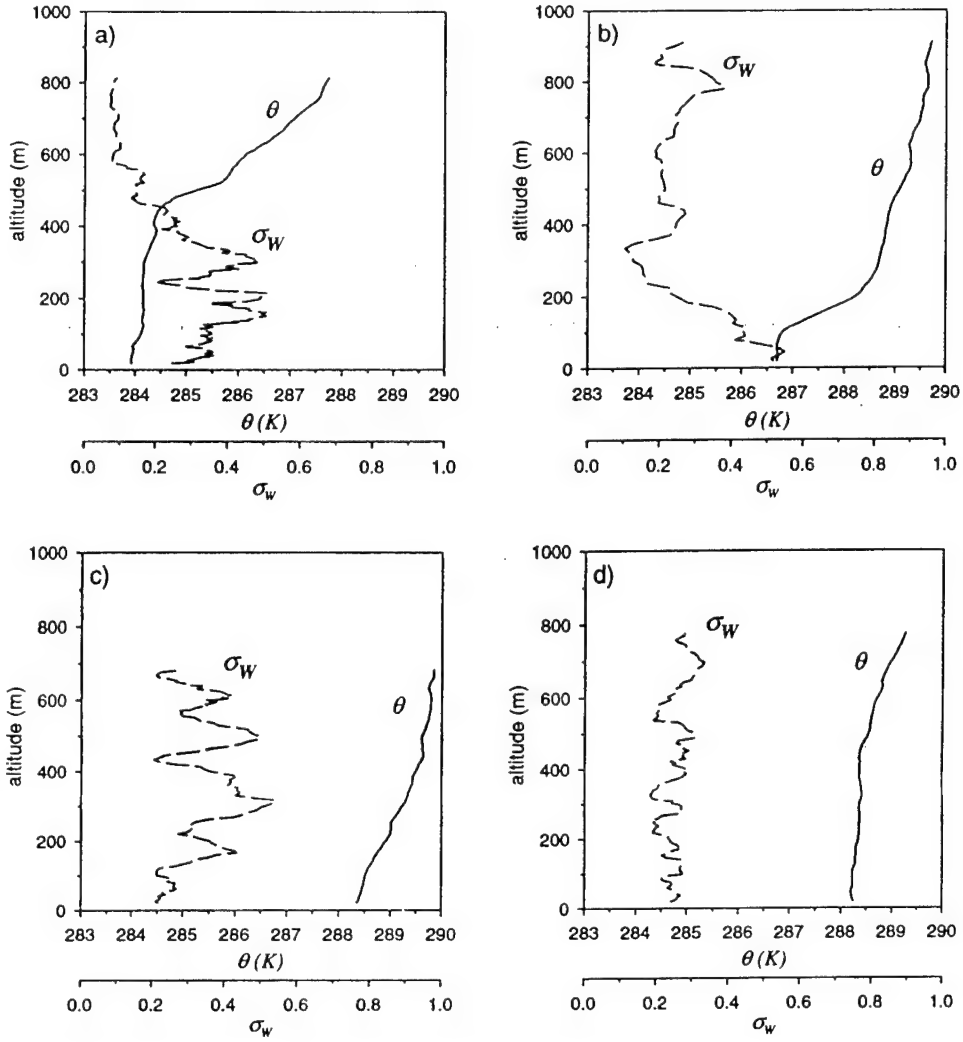

Figure 7. Example slant aircraft soundings of potential temperature and the standard deviation of vertical velocity for November 3, 1997.

than the sea surface. The standard deviation of vertical velocity constructed from slant soundings is noisy because of inadequate sampling at a given level and because of contamination of the computed perturbations by variations of the mean flow within the averaging window of 1 km, as the aircraft ascends and descends. Such errors artificially prevent the standard deviation of vertical velocity from reaching very small values. With a typical ascent rate of 2%, the 1-km averaging length corresponds to a vertical elevation change of 20 m. The sequential soundings indicate a variety of boundary layer structures, and the boundary layer is sometimes poorly defined. The thin, cool boundary layer is observed in only some of the soundings and in other cases may be confined to below the lowest observation level of about 30 m. A few examples are included in Figure 7. Figure 7a shows a deep 400-m boundary layer, while Figure 7b shows a thinner, well-defined boundary layer with significant turbulence over a depth of 100 m. Figure 7d might correspond to a deep boundary layer, while the boundary layer cannot be readily defined in Figure 7c.

Surprisingly, the vertical structure did not seem to vary systematically with offshore distance, suggesting more than one collapse and recovery sequence. The stability on this day is substantially weaker than that for the ultrasmooth case on March 6, 1999, discussed above. The sequential soundings indicate that individual soundings on this day would be misleading and that the evolution and elimination of the stable internal boundary layer may be intermittent. As one possible explanation, accelerating flow above the thin, cool stable layer enhances the shear and induces mixing (boundary-layer recovery), which in turn reduces the shear and increases the Richardson number. This would lead to decay of turbulence and reformation of the cool stable layer adjacent to the surface. Unsteadiness of the upstream wind may also be a factor, particularly since the fetch at a given point is sensitive to wind direction.

7. Roughness Length Dependence on Stability

The aerodynamic roughness length generally decreases with increasing bulk Richardson number except for the most stable conditions (Figure 8). For the calculations in Figures 8 and 9, a lower threshold of 10^{-10} m was imposed on the roughness length to restrict the range of the vertical axis. Roughness lengths this small are probably zero within observational error. Therefore mean values in Figures 8 and 9 approaching 10^{-10} m

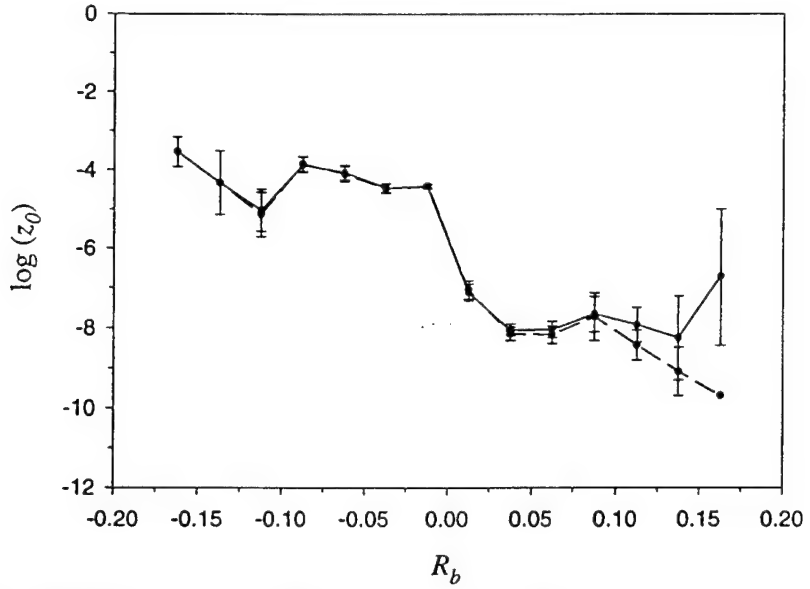

Figure 8. The dependence of the aerodynamic roughness length on the bulk Richardson number for November–December 1999 (solid line) and after removing cases with downward transport of vertical velocity variance (dashed line). Vertical brackets indicate the standard error.

imply that the roughness length is zero within observational error for many of the cases comprising the average.

Large values of the roughness length for very stable conditions occasionally occur with downward transport of vertical velocity variance toward the surface. Removal of these cases reduces the averaged value of the roughness length for very stable conditions, in which case the roughness length decreases with increasing stability. Since the turbulence in cases of downward transport of turbulence energy is not completely controlled by surface fluxes and z/L, Monin-Obukhov similarity theory may not apply. Then the aerodynamic roughness loses its physical meaning.

The roughness length (and the neutral drag coefficient) reaches a minimum value around 5 m s^{-1} (Figure 9), as is observed in numerous previous studies. This minimum value is thought to occur because of the combination of increasing roughness with increasing wind speed and special effects at weak winds. The special effects for weak winds include the role of surface tension and surfactants, transport by boundary-layer scale convective eddies, and "wave-induced" stress associated with swell.

We require that the stress vector be directed within 45 degrees of opposing the wind vector (section 3) to reduce the contribution of the swell to the composited roughness length.

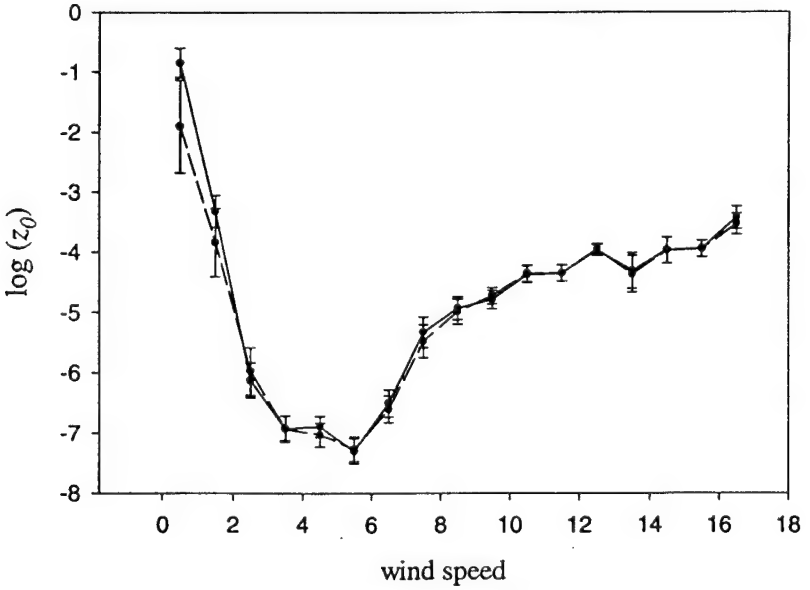

Figure 9. The dependence of the roughness length on wind speed for the November–December 1999 LongEZ data (dashed) and after removing restrictions on the stress direction (section 3) (solid). Vertical brackets indicate the standard error.

Relaxing this criteria (Figure 9, solid line) modestly increases the roughness length (and drag coefficient) at weak wind speeds but has little effect at other wind speeds. Therefore it is likely that part of the increase of the roughness length at weak wind speeds is due to wave-driven stress. The wave-driven stress is not expected to obey Monin-Obukhov similarity theory but enhances the stress and therefore the aerodynamic roughness length computed from that stress.

For weak wind stable conditions, longer waves exert an important influence on the stress, as was observed by *Plant et al.* [1999]. In fact, in their case the stress was nearly constant as the wind decreased to values below a few meters per second. *Rieder and Smith* [1998] find that the wave-induced part of the stress does not vanish as the wind vanishes, causing the drag coefficient to become large. However, they also find that even after attempting to remove the wave-driven stress, some increase of the drag coefficient at weak winds remains. *Mahrt et al.* [1996] found that the increase of the drag coefficient at weak wind speeds over the water is very sensitive to the method of calculation. *Mahrt et al.* [2001] show that the roughness length increases at weak winds speeds also over land surfaces, even over bare ground, alluding to meandering of the wind and stress vectors as a contributing factor.

These weak wind effects contribute to the dependence of the roughness length on stability since the stability tends to increase with decreasing wind speed. However, the present analysis (Figure 9) indicates that the roughness lengths are smallest for a combination of stable conditions and wind speeds in the range of 3–5 m s^{-1}. For winds greater than 6 m s^{-1}, the roughness length increases with increasing wind speed. This increase is due to near-neutral and unstable cases. The roughness length does not increase with wind speed for stable conditions.

8. Conclusions

The above analysis of LongEZ aircraft data and sonic anemometer data reveals frequent occurrence of very small surface stress and roughness lengths. These very small roughness lengths with near collapse of the turbulence are generally associated with advection of warmer air from land over colder water. Numerical estimates of the aerodynamic roughness length may be subject to large errors for weak surface fluxes in very thin boundary layers (section 3) because of significant random flux errors, systematic small-scale flux loss, errors due to fluctuations of the aircraft altitude, and errors in the estimated wind speed by the aircraft. With very thin, stable boundary layers, the stress may decrease significantly between the surface and the observational level. In this case, Monin-Obukhov similarity theory does not apply at the observation level, and the roughness length computed from the data must compensate for this inapplicability. Here "quasi-frictional decoupling" refers to very small values of the surface stress and roughness length and/or extremely thin atmospheric boundary layers. In spite of the above observational difficulties, the small values of the momentum flux inferred from the aircraft data also occur with sonic anemometer data collected from buoys and a tower at the end of a 570-m pier. Ultrasmooth values of the aerodynamic roughness length do not necessarily imply specific information on the wave state. The value of the aerodynamic roughness length only provides the correct flux given the specified stability functions (section 2), and its relationship to wave state in these cases is uncertain [*Sun et al.*, 2001].

The influence of warm air advection extends the influence of land off the coast for tens of kilometers or more. The very small roughness lengths for stable conditions are partly due to reduction of the downward momentum flux by the stable stratification. The data also show the usual minimum of the roughness length and neutral drag coefficient for wind speeds of about 5 m s^{-1}. The larger values of the roughness length at weaker wind speeds are partly associated with large deviations of the stress direction from opposite the wind vector, apparently due to the influence of swell. The very small roughness lengths are most likely to occur with a combination of intermediate wind speeds and stable stratification. Significant wind speed is required here to maintain the advection of warmer air over the cooler sea.

In some stable cases the vertical transport of turbulence may be downward, implying that the main source of turbulence is above the surface-based stable layer. In these cases the aerodynamic roughness length is much larger than that for the usual case of upward transport of turbulence energy. The multitude of physical influences on the surface stress and the difficulty of measuring weak momentum fluxes prevent categorical conclusions.

Acknowledgments. We gratefully acknowledge Jeff French, Ed Dumas, and Chris Vogel for important contributions to the three field programs. Will Drennen provided the data from the Romeo buoy. Bill Birkemeier and Gene Bichner of the U.S. Army Corps of Engineers Field Research Facility at Duck, North Carolina, are acknowledged for their helpful assistance. This material is based upon work supported by grants N00014-97-1-0279, N00014-98-1-0245, and N00014-97-F-0123 from the Office of Naval Research, Marine Meteorology.

References

Charnock, H., Wind stress over a water surface, *Q. J. R. Meteorol. Soc.*, *81*, 639–640, 1955.

Crescenti, G. H., T. L. Crawford, and E. J. Dumes, Data report: Long EZ(N3R) participation in the 1999 Shooling Waves Experiment (SHOWEX) pilot study, *Tech. Memo. ERL ARL-232*, Natl. Oceanic and Atmos. Admin., Silver Spring, Md., 1999.

Donelan, M. A., Air-sea interaction, in *Ocean Engineering Science*, edited by B. LeMehaute and D. M. Hanes, pp. 239–292, John Wiley, New York, 1990.

Dyer, A. J., A review of flux-profile relationships, *Boundary Layer Meteorol.*, *7*, 363–372, 1974.

Edson, J., and C. W. Fairall, Similarity relationships in the marine atmospheric surface layer for terms in the TKE and scalar variance budgets, *J. Atmos. Sci.*, *55*, 2311–2328, 1998.

Frederickson, P. A., and K. L. Davidson, Air-sea flux measurements from a buoy in a coastal ocean region, in *Fourteenth Symposium on Boundary Layers and Turbulence*, pp. 530–533, Am. Meteorol. Soc., Boston, Mass., 2000.

Freilich, M., and R. Dunbar, The accuracy of the NSCAT 1 vector winds: Comparisons with National Data Buoy Center buoys, *J. Geophys. Res.*, *104*, 11,231–11,246, 1999.

French, J. R., G. H. Crescenti, T. L. Crawford, and E. J. Dumas, Long EZ participation in the 1999 Shooling Waves Experiment (SHOWEX), *Data Rep. OAR ARL-20*, Natl. Oceanic and Atmos. Admin., Silver Spring, Md., 2000.

Geernaert, G. L., S. E. Larsen, and F. Hansen, Measurements of the wind stress, heat flux, and turbulence intensity during storm conditions over the North Sea, *J. Geophys. Res.*, *92*, 127–139, 1987.

Grachev, A., and C. Fairall, Upward momentum transfer in the marine boundary layer, *J. Phys. Oceanogr.*, *31*, 1698–1711, 2001.

Howell, J., and L. Mahrt, Multiresolution flux decomposition, *Boundary Layer Meteorol.*, *83*, 117–137, 1997.

Kahma, K., and M. Donelan, A laboratory study of the minimum wind speed for wind wave generation, *J. Fluid Mech.*, *192*, 339–364, 1987.

Kitaigorodski, S., and M. Donelan, Wind-wave effects on gas transfer,

in *Gas Transfer at Water Surfaces*, edited by W. H. Brutsaert and J. Jirka, pp. 147–170, D. Reidel, Norwell, Mass., 1984.

Maat, N., C. Kraan, and W. A. Oost, The roughness of wind waves, *Boundary Layer Meteorol.*, *54*, 89–103, 1991.

Mahrt, L., D. Vickers, J. Howell, J. Edson, J. Hare, J. Højstrup, and J. Wilczak, Sea surface drag coefficients in RASEX, *J. Geophys. Res.*, *101*, 14,327–14,335, 1996.

Mahrt, L., D. Vickers, J. Edson, J. Wilczak, J. Hare, and J. Højstrup, Boundary-layer transitions in offshore flow, *Boundary Layer Meteorol.*, *100*, 3–46, 2001.

Moller, D., P. Mourad, and S. Frasier, Field observations of radar backscatter from the ocean surface under low wind speed conditions, *J. Geophys. Res.*, *105*, 24,059–24,069, 2000.

Nordeng, T. E., On the wave age dependent drag coefficient and roughness length at sea, *J. Geophys. Res.*, *96*, 7167–7174, 1991.

Paulson, C. A., The mathematical representation of wind speed and temperature profiles in the unstable atmospheric surface layer, *J. Appl. Meteorol.*, *9*, 857–861, 1970.

Perrie, W., and B. Toulany, Fetch relations for wind-generated waves as a function of wind-stress scaling, *J. Phys. Oceanogr.*, *20*, 1666–1681, 1990.

Piccirillo, P., and C. Van Atta, The evolution of a uniformly sheared thermally stratified turbulent flow, *J. Fluid Mech.*, *314*, 61–86, 1997.

Plant, W., W. Keller, V. Hesany, K. Hayes, K. Hoppel, and T. Blanc, Measurements of the marine boundary layer from an airship, *J. Atmos. Oceanic Technol.*, *15*, 1433–1458, 1998.

Plant, W., D. Weissman, W. Keller, V. Hessany, K. Hayes, and K. Hoppel, Air/sea momentum transfer and the microwave cross section of the sea, *J. Geophys. Res.*, *104*, 11,173–11,191, 1999.

Rieder, K. F., and J. A. Smith, Removing wave effects from the wind stress vector, *J. Geophys. Res.*, *103*, 1363–1374, 1998.

Smedman, A.-S., H. Bergström, and B. Grisogano, Evolution of stable internal boundary layers over a cold sea, *J. Geophys. Res.*, *102*, 1091–1099, 1997a.

Smedman, A.-S., U. Hogström, and H. Bergström, The turbulence regime of a very stable marine airflow with quasi-frictional decoupling, *J. Geophys. Res.*, *102*, 21,049–21,059, 1997b.

Smedman, A., U. Hogström, and H. Bergström, The marine atmospheric boundary layer during swell, according to recent studies in the Baltic Sea, in *Air-Sea Exchange: Physics, Chemistry and Dynamics*, edited by G. L. Geernaert, pp. 175–196, Kluwer Acad., Norwell, Mass., 1999.

Sun, J., D. Vandemark, L. Mahrt, D. Vickers, T. Crawford, and C. Vogel, Momentum transfer over the coastal zone, *J. Geophys. Res.*, *106*, 12,437–12,448, 2001.

Toba, Y., and M. Koga, A parameter describing overall conditions of wave breaking, white capping, sea-spray production and wind stress, in *Oceanic Whitecaps*, edited by E. C. Monahan and G. Mac Niocaill, pp. 37–47, D. Reidel, Norwell, Mass., 1986.

Vickers, D., and L. Mahrt, Fetch limited drag coefficients over shallow water, *Boundary Layer Meteorol.*, *89*, 53–79, 1997a.

Vickers, D., and L. Mahrt, Quality control and flux sampling problems for tower and aircraft data, *J. Atmos. Oceanic Technol.*, *14*, 512–526, 1997b.

Vickers, D., and L. Mahrt, Observations of nondimensional shear in the coastal zone, *Q. J. R. Meteorol. Soc.*, *125*, 2685–2702, 1999.

Vickers, D., L. Mahrt, J. Sun, and T. Crawford, Structure of off-shore flow, *Mon. Weather Rev.*, *129*, 1251–1258, 2001.

Weissman, D., and H. Graber, Satellite scatterometer studies of ocean surface stress and drag coefficients using a direct model, *J. Geophys. Res.*, *104*, 11,329–11,335, 1999.

Wilczak, J. M., J. Edson, J. Højstrup, and T. Hara, The budget of turbulence kinetic energy in the marine atmosphere, in *Air-Sea Exchange: Physics, Chemistry and Dynamics*, edited by G. Geernaert, pp. 153–174, Kluwer Acad., Norwell, Mass., 1999.

Winstead, N., and G. Young, An analysis of exit flow drainage jets over the Chesapeake Bay, *J. Appl. Meteorol.*, *39*, 1269–1281, 2000.

T. L. Crawford and G. Crescenti, NOAA Air Resources Laboratory, Idaho Falls, ID 83402, USA.

P. Frederickson, Naval Postgraduate School, Monterey, CA 93943, USA.

L. Mahrt and D. Vickers, College of Oceanic and Atmospheric Sciences, Oregon State University, Corvallis, OR 97331, USA. (mahrt@oce.orst.edu)

J. Sun, National Center for Atmospheric Research, Boulder, CO 97331, USA.

(Received November 13, 2000; revised May 18, 2001;
accepted May 21, 2001.)

Structure of Offshore Flow

DEAN VICKERS AND L. MAHRT

College of Oceanic and Atmospheric Sciences, Oregon State University, Corvallis, Oregon

JIELUN SUN

National Center for Atmospheric Research, Boulder, Colorado

TIM CRAWFORD

NOAA/FRD, Idaho Falls, Idaho

(Manuscript received 25 April 2000, in final form 1 September 2000)

ABSTRACT

The horizontal and vertical structure of the mean flow and turbulent fluxes are examined using aircraft observations taken near a barrier island on the east coast of the United States during offshore flow periods. The spatial structure is strongly influenced by the surface roughness and surface temperature discontinuities at the coast. With offshore flow of warm air over cool water, the sea surface momentum flux is large near the coast and decreases rapidly with increasing offshore distance or travel time. The decrease is attributed to advection and decay of turbulence from land. The rate of decrease is dependent on the characteristic timescale of the eddies in the upstream land-based boundary layer that are advected over the ocean. As a consequence, the air–sea momentum exchange near the coast is influenced by upstream conditions and similarity theory is not adequate to predict the flux.

The vertical structure reveals an elevated layer of downward momentum flux and turbulence energy maxima over the ocean. This increase in the momentum flux with height contributes to acceleration of the low-level mean wind. In the momentum budget, the vertical advection term, vertical flux divergence term, and the horizontal pressure gradient term are all of comparable magnitude and all act to balance large horizontal advection. An interpolation technique is applied to the aircraft data to develop fetch–height cross sections of the mean flow and momentum flux that are suitable for future verification of numerical models.

1. Introduction

In quasi-stationary atmospheric flow over a homogeneous surface, Monin–Obukhov similarity theory and bulk flux formula have successfully predicted turbulent surface fluxes over the sea (e.g., Fairall et al. 1996; Högström 1996). Here quasi-stationary means that the total time rate of change of turbulent quantities is small compared to production and dissipation terms. However, in regions of significant surface heterogeneity, such as near coastlines, advection by the mean wind and vertical flux divergence can become significant. In this case, a well-defined surface layer may not exist, and similarity theory will be inadequate due to a dependence of the fluxes on upstream conditions.

With offshore flow, the turbulence advected from land must adjust to the new aerodynamically smoother sea surface and new surface temperature. A conceptual model of this adjustment is internal boundary layer theory (Garratt 1990). The internal boundary layer (IBL) is the region near the surface where the flow is directly influenced by the new underlying surface. While unstable IBLs (e.g., cool air over warm water) have a well-defined convective growth mechanism due to the surface heat flux, the stable case is more complex and less well understood. In the stable case, the residual land-based turbulence advected downwind above the stable IBL may be stronger than the turbulence within the IBL, leading to an increase in turbulence kinetic energy (TKE) with height. This occurs despite the fact that the residual turbulence generated over land decays through dissipation as it is advected over the water. This stable case is not described by traditional IBL theory (Mahrt et al. 2001).

Advection and decay of convective turbulence were studied by Nieuwstadt and Brost (1986) by abruptly switching off the upward surface heat flux in a large-

Corresponding author address: Dean Vickers, College of Oceanic and Atmospheric Sciences, Oceanography Admin. Bldg. 104, Oregon State University, Corvallis, OR 97331-5503.
E-mail: vickers@oce.orst.edu

eddy simulation model. They found that the relevant scaling parameters of the decay of TKE were the convective velocity scale w_* and the mixed layer depth h. Sorbjan (1997) extended the modeling approach by imposing a gradual rather than a sudden time change in the surface heat flux. Studies reviewed in Monin and Yaglom (1975) suggest that the integral length scale of decaying turbulence increases with time due to finescale eddies decaying first. The influence of advection of covariances by the mean wind on the measured flux is sometimes viewed in terms of the flux footprint approach. With strong winds, the footprint may extend a considerable distance in the upwind direction (Horst and Weil 1994). This situation is further complicated by the fact that the eddies associated with the land-based fluxes decay through dissipation and that the momentum fluxes are influenced by pressure fluctuations, neither of which are included in footprint theory.

In the coastal region, the sea surface momentum flux can also be influenced by shoaling waves and young growing gravity wave fields on the ocean surface. With shoaling waves, wave breaking and wave steepening can augment the momentum flux (Banner 1990). Wind–wave interaction leading to development of new (young) waves can augment the momentum flux compared to conditions with older wave fields that are more in equilibrium with the wind (Geernaert et al. 1987; Donelan 1990).

Numerous authors have reported evidence of marine low-level jets in offshore flow (e.g., Smedman et al. 1993 and references therein). They propose that the jet is formed due to an inertial oscillation caused by frictional decoupling from the surface when warm air flows over cooler water. The decoupling occurs because the turbulence near the surface collapses partly due to buoyancy destruction. Smedman et al. (1993) make an analogy between the spatial structure of the marine jet and the more well known nocturnal jet over land.

In this work, we investigate the spatial structure of the mean flow, momentum flux, heat flux, and TKE in the first 10 km offshore as land-based turbulence is advected over the water, influenced by the new smoother sea surface, and modified by the stratification. For stable conditions, we relate the timescale associated with the observed decrease in the sea surface momentum flux with travel time from the coast to a decay timescale characteristic of the turbulence in the boundary layer over land. Individual terms in the equation of motion for the mean wind are examined. The data description and analysis methods are discussed in the next section. Our results and conclusions follow.

2. Data

This study analyzes observations from the Atlantic coast near Duck, North Carolina, on the Outer Banks barrier island (Fig. 1) during 2–18 March 1999 and 11 November–4 December 1999 during the Shoaling Waves Experiment (SHOWEX) (Sun et al. 2001). The roughness elements on the Outer Banks consist of multistory vacation homes and commercial buildings. Despite the short fetch over land due to the narrowness of the Outer Banks, significant mixing is generated near the surface over land due to these large roughness elements and solar heating of the surface.

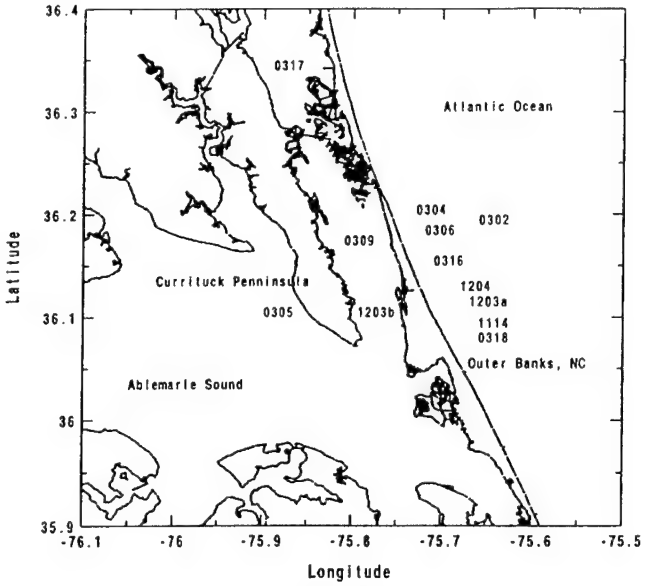

FIG. 1. SHOWEX study area near Duck, NC, and the location and date (mmdd) of the 12 offshore flow case studies. The mean flow is from the SW in all cases except 0305 and 0309 when it is from the NE. The upstream land is the Outer Banks in all cases except 0317, 0305, and 1203b when it is Currituck Peninsula.

The National Oceanic and Atmospheric Administration (NOAA) LongEZ (N3R) aircraft measured the three components of the wind, air temperature, humidity, surface temperature, and atmospheric pressure. With clean aerodynamics and a pusher configuration, the LongEZ is an ideal platform for low-and-slow air surface exchange measurements. The wind components were measured using the BAT turbulence probe designed and built in collaboration with Airborne Research Australia (Crawford and Dobosy 1992). Information from Trimble Advanced Navigation Systems differential Global Positioning System receivers are extended to high frequencies by accelerometers to determine position and platform attitude. The air temperature was measured using a Victory Engineering Corp. microbead thermistor. Surface radiative temperature was measured with an Everest Inter-science Inc. 4000.4GL instrument.

The aircraft flight patterns considered in this work include repeated tracks close to and parallel to the coast for a sequence of offshore distances and heights, as well as repeated tracks perpendicular to the coast for a sequence of different altitudes. The same flight track was flown numerous times to ensure adequate statistics and reduce the random flux sampling errors associated with a single pass of the track. The lowest-level aircraft flights over water were flown between 10 and 20 m.

a. Derived quantities

All derived fields were calculated from quality controlled aircraft flux legs. The original flight legs were first examined to test for the suitability of calculating fluxes with the eddy correlation method. Portions of the leg satisfying criteria for constant altitude and small aircraft roll, pitch, and heading angle changes were considered potential flux legs. The potential flux legs were then subjected to a quality control software package designed to detect and eliminate instrument and data recording problems (Vickers and Mahrt 1997).

Turbulence was defined to include all fluctuations on length scales from 1 km down to the resolution of the instruments (approximately 1 m based on a 50-Hz sampling rate and a typical aircraft ground speed of 50 m s^{-1}). Sensitivity studies testing the length scale dependence of the calculated fluxes showed that a 1-km length scale was sufficient to capture most of the turbulent flux. Derived quantities include the friction velocity, mean wind speed, and TKE:

$$u_{*l} = (\overline{w'u'}^2 + \overline{w'v'}^2)^{1/4}, \quad (1)$$

$$U = (\overline{u}^2 + \overline{v}^2)^{1/2}, \quad \text{and} \quad (2)$$

$$\text{TKE} = 0.5(\overline{u'u'}^2 + \overline{v'v'}^2 + \overline{w'w'}^2), \quad (3)$$

where primes denote fluctuations from a 1-km mean and overbars represent a 1-km average. Here, u_{*l} refers to the local value of the friction velocity at height z.

b. Interpolation method

We interpolate the 1-km data onto a fetch–height (x, z) grid of resolution $\Delta x = 500$ m and $\Delta z = 25$ m with a domain equal to 0–10-km fetch and 10–310 m in height. Fetch is distance over the ocean that an air parcel has traveled since leaving land and is a function of aircraft position, coastal geometry, and wind direction. Quantity ϕ at a grid point was calculated as

$$\phi(x, z) = \frac{\sum w_k \phi_k}{\sum w_k}, \quad (4)$$

where the sum is over all 1-km mean data points and ϕ represents u_{*l}, U, TKE, or the heat flux. The weights (w_k) are assigned inversely proportional to the distance between the observations and the grid point as

$$w_k = \frac{2 - \zeta}{2 + \zeta} \quad \text{and} \quad (5)$$

$$\zeta = \frac{(x_k - x)^2}{X^2} + \frac{(z_k - z)^2}{Z^2}, \quad (6)$$

and we select $X = 3\Delta x$, $Z = 3\Delta z$. For those observations where $|x_k - x| > X$ or $|z_k - z| > Z$, the weight is set to zero; that is, X and Z define a maximum region of influence. The length of time between the first and last aircraft observations included in an individual cross section was approximately 1 h and varied slightly between cases (Table 1). The profile at the coastline ($x = 0$) was calculated as the average of the mean profile over land for the longest land fetches available and the interpolated profile for zero fetch using the segments over the ocean.

TABLE 1. Offshore flow case studies (see Fig. 1 for locations). Mean wind speed, friction velocity, and heat flux are the interpolated values at $x = 0$ (coastline) and $z = 35$ m. Values in parentheses are estimates of the standard error. Asterisks indicate cases with only low-level data.

Date (mmdd)	Time (UTC)	U (m s^{-1})	u_{*l} (m s^{-1})	$\overline{w'\theta'}$ (m s^{-1} °C)
0302	2000	5.7 (0.3)	0.27 (0.04)	0.009 (0.004)
0305	1830	4.5 (0.1)	0.51 (0.03)	0.125 (0.015)
0317	1900	5.0 (0.1)	0.44 (0.02)	0.003 (0.003)
0318	1530	6.5 (0.2)	0.71 (0.02)	0.041 (0.004)
1114	1800	7.1 (0.3)	0.55 (0.02)	0.027 (0.006)
1203a	1330	7.9 (0.3)	0.27 (0.03)	−0.010 (0.012)
1203b	1330	6.0 (0.3)	0.30 (0.06)	−0.014 (0.005)
0304*	1600	12.1 (1.1)	0.46 (0.09)	0.035 (0.013)
0306*	1500	5.7 (0.2)	0.43 (0.03)	0.002 (0.004)
0309*	1530	6.3 (0.3)	0.31 (0.02)	0.020 (0.001)
0316*	1930	4.9 (0.2)	0.45 (0.02)	0.044 (0.011)
1204*	1800	6.2 (0.2)	0.51 (0.02)	0.005 (0.003)

In the interpolation, all information contained in the data was used to extract the spatial structure of the mean. An alternative method, where the data were grouped (binned) into fetch and altitude categories, was employed to obtain the variance, from which we estimated a sampling error. We calculated the standard error for the mean estimates in Table 1 (at $x = 0$ and $z = 35$ m) by combining all observations below 70-m altitude over land and below 50-m altitude over the first 500 m of water fetch. This standard error is an overestimate of the standard error associated with purely random sampling errors due to the unavoidable inclusion of coherent spatial variability in the sample.

The kinematic sea surface momentum flux (u_*^2), which represents the air–sea exchange of momentum, was estimated by linearly extrapolating the interpolated estimates at heights of 10 and 35 m to the surface. In the stable case, where the momentum flux typically increases with height close to the coast, the extrapolation yields an estimate of u_*^2 that is smaller than the estimate at the lowest aircraft measurement height.

c. Residual turbulence timescale

To characterize the residual turbulence that is generated over land and advected over the ocean, we calculate a turbulence timescale. In traditional scaling arguments, the turnover time for a large eddy is proportional to L_s/σ_w, where σ_w is the standard deviation of the vertical wind defined for some suitable averaging time, and L_s is the length scale where 50% of the total variance of the vertical wind occurs at smaller scales. Here, L_s is strongly correlated with the length scale of the peak of the spectra. To estimate L_s, we applied multi-

resolution decomposition (Howell and Mahrt 1997) to the vertical velocity data obtained in the boundary layer over land. The spectra from repeated flight tracks in the same region on the same day were composited by averaging the estimates of L_s for individual passes.

d. Evaluating gradients

The equation of motion for the mean wind is written as

$$\frac{\partial U}{\partial t} + U\frac{\partial U}{\partial x} + W\frac{\partial U}{\partial z} + \frac{\partial \overline{w'u'}}{\partial z} + \frac{\partial \overline{u'u'}}{\partial x} = -\frac{1}{\rho}\frac{\partial P}{\partial x}, \quad (7)$$

where we have neglected terms involving horizontal gradients in the direction parallel to the coast. The terms in Eq. (7) were estimated using finite differences evaluated across a conceptual grid box extending from 1 to 3 km in fetch and from 10 to 135 m in height above the water. Horizontal gradients were computed as the difference of the vertical averages over the grid box, and vertical gradients were computed as the difference of horizontal averages. A sequence of sensitivity studies, where the grid box was moved farther downstream and made larger in the x direction, showed that while the exact magnitude of the terms is sensitive to the region considered, the relative magnitude and sign of the terms are not sensitive. The local time rate of change term ($\partial U/\partial t$) was estimated from the earliest and latest aircraft passes, which were typically 1 h apart.

The mean vertical velocity (W) in the vertical advection term was estimated by first removing the flight-average vertical velocity from the 1-km means. A surprisingly coherent pattern was observed in which the mean vertical motion was downward (upward) in the region of acceleration (deceleration) of the horizontal mean wind. Deceleration of the mean wind and mean rising motion were commonly observed over land, while acceleration of the mean wind and mean sinking motion were found in the first few kilometers downwind from the coast in stable conditions. For the longest sea fetches, the mean vertical motion was small downward.

Attempts to calculate the horizontal pressure gradient by removing the altitude dependence of the pressure as measured by the aircraft were deemed unreliable. As an alternative, we estimated the local horizontal pressure gradient due only to the local horizontal temperature gradient using the hydrostatic equation and the observed temperature field from the aircraft measurements. An estimate of the large-scale horizontal pressure gradient was calculated from the NCEP–NCAR reanalysis surface pressure (Kalnay et al. 1996). The reanalysis is a joint project between the National Centers for Environmental Prediction (NCEP) and the National Center for Atmospheric Research (NCAR). The analyzed surface pressure from the model was interpolated in time and space for each case study.

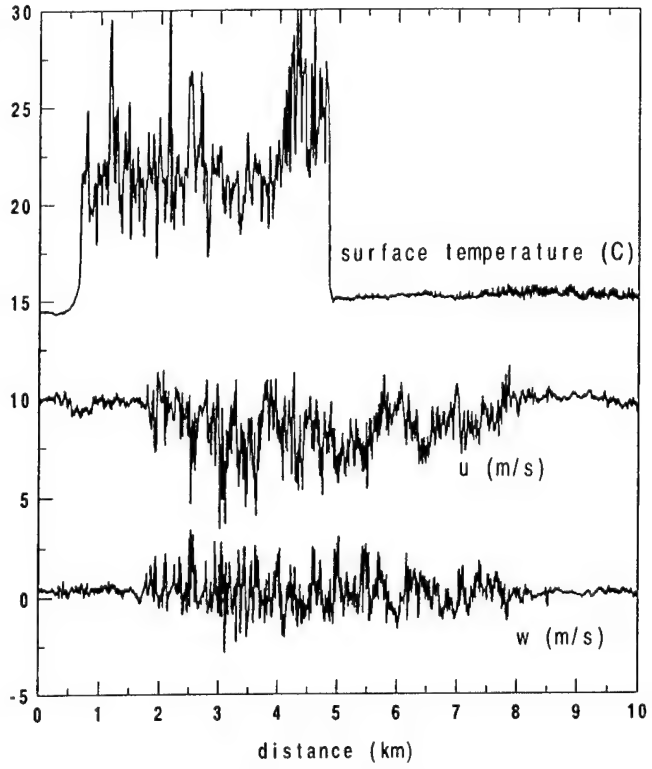

FIG. 2. Surface radiative temperature (°C), horizontal wind speed (m s^{-1}), and vertical wind speed (m s^{-1}) as a function of distance (km) for one aircraft flux leg at 110-m altitude on 1114 as the aircraft travels west to east from over Albemarle Sound (left edge), over the Outer Banks (the warm region), and then over the Atlantic Ocean. The mean flow direction is westerly.

3. Spatial variation

Time series from a single aircraft leg crossing the Outer Banks is shown in Fig. 2. Unlike in the cross sections, in this example the wind components are not time averaged, interpolated, or smoothed. The two coastlines are clearly distinguished by the surface radiative temperature. The stable air–sea temperature difference is 6° to 8°C. The aircraft intersects a convective land-based IBL with strong turbulence at 1.1 km inland from the windward coastline. The turbulence generated over land is advected downwind over the ocean where the wind fluctuations decrease in strength until beyond 4 km, or 8 min travel time, where the turbulence becomes very weak. The 1-km average wind speed is reduced from 10 m s^{-1} over the sound on the windward side of land to 8 m s^{-1} over the leeward side of land. Over the Atlantic, the mean flow accelerates back to its original upstream value by the time that the residual land-based turbulence has collapsed. In the remainder of this section, we discuss case studies of composite fetch–height cross sections in offshore flow (Table 1 and Fig. 1). These case studies provide challenging situations for future attempts to model offshore flow.

Case 0318 (Fig. 3) is downwind of the Outer Banks over the Atlantic, where the air temperature is initially 8°C warmer than the sea surface temperature. Based on

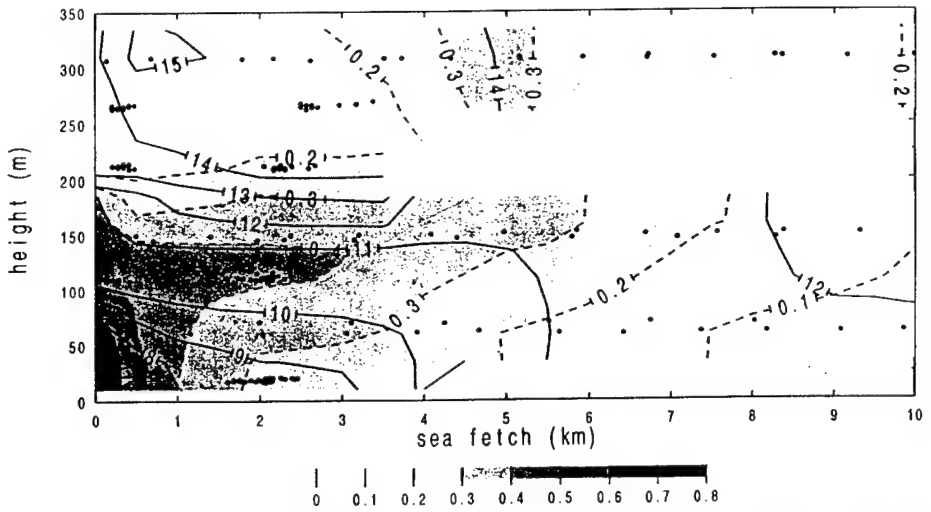

FIG. 3. Fetch–height cross sections for case 0318 of the friction velocity (shaded and dotted contours, m s^{-1}) and the mean wind speed (solid contours, m s^{-1}). Dots indicate locations of the 1-km data points used in the interpolation. Clusters of data points result from the parallel flight tracks.

the decrease in mean TKE with height over land (not shown), the depth of the land-based convective IBL at the leeward coastline after 4.8 km of land fetch is approximately 200 m. Beyond 1 km from the coast, strong residual turbulence advected from land becomes partially detached from the surface leading to a downward momentum flux (and TKE) maxima aloft. Mahrt et al. (2001) observed similar vertical structure of stable offshore flow from tower data off the Danish coast; however, the air–sea temperature difference of the present offshore flow is larger and the vertical structure is more persistent. We attribute the elevated flux maxima to a combination of several factors: (a) more dissipation of the residual turbulence at lower levels due to smaller mean eddy size near the surface, (b) more buoyancy destruction of turbulence at lower levels over the ocean due to the closer proximity to the cold water, and (c) shorter travel time at higher levels, for a given fetch distance, due to the stronger mean wind aloft. Cases 1114 (Fig. 4) and 0317 (Fig. 5) are similar in many respects to case 0318. In all three of these stable offshore flow cases, an elevated layer of momentum flux and TKE maxima is observed along with acceleration of the low-level mean wind in the first several kilometers over the water.

In case 1203a, a shallow (<50-m depth) convective IBL develops over the Atlantic in response to cold air advection from land. The air is 3°C colder than the water. Beyond 1 km from the coast, the sea surface momentum flux is constant with fetch and the momentum flux slowly decreases with height (Fig. 6). This unstable case is quite different from the stable case, which included a rapid decrease in the sea surface momentum flux with fetch, an increase in the momentum flux with height, and acceleration of the low-level mean wind.

The remaining case studies (not shown) clearly demonstrate the strong influence of stability (air–sea temperature difference) on the fetch dependence of the sea surface momentum flux. For unstable conditions, in which buoyancy generation of turbulence over the warm water is significant, the sea surface momentum flux is nearly independent of fetch beyond the first kilometer offshore. For stable flow of warm air over cool water, the momentum flux decreases rapidly in the first several kilometers and gradually approaches a constant value after 6–10 km of fetch.

4. Advective-decay timescale

In this section, we test a prediction for the travel-time dependence of the sea surface momentum flux based on a characteristic timescale of the turbulence in the upstream boundary layer over land. The hypothesis is that local generation of momentum flux over the ocean for short fetch is small compared to the influence due to advection of strong turbulence from land in stable offshore flow. Cases with convective conditions over the water, where local buoyancy generation of turbulence is significant, were excluded.

We calculated an advective-decay rate that describes the observed decrease in the sea surface momentum flux with increasing travel time from the coast. From a Lagrangian viewpoint, the advective-decay rate in stable offshore flow is at least partly due to viscous dissipation of the Reynolds stress. Based on the actual travel-time dependence (Fig. 7), we formulated the sea surface momentum flux as a function of travel time t from the coast as

$$u_*^2(t) = u_{*o}^2 \exp(-t/\tau) + u_{*eq}^2[1 - \exp(-t/\tau)], \quad (8)$$

where τ is the advective-decay timescale, u_{*eq} is the equilibrium value of u_* for long travel time over the water beyond the influence of advection from land, and

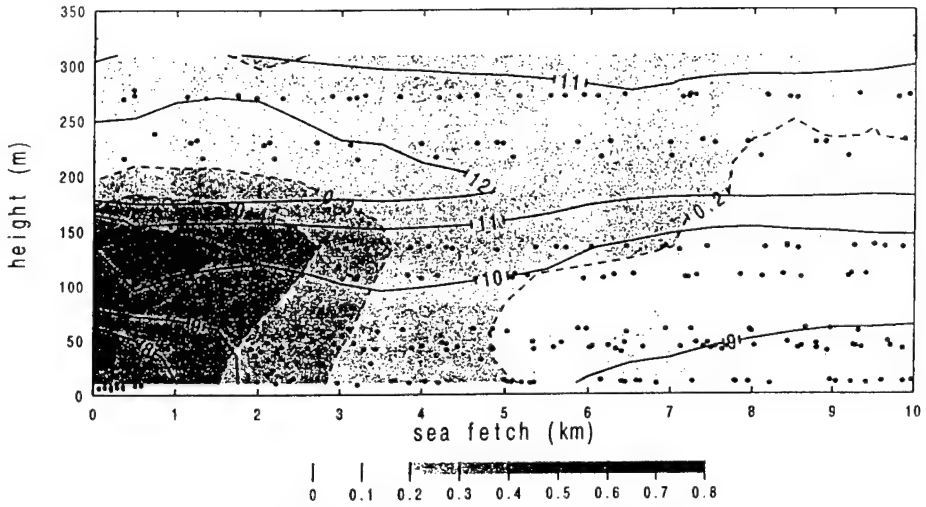

FIG. 4. Same as Fig. 3 except for case 1114.

u_{*o} is the initial value at the coast. The timescale τ was calculated for each case study by applying linear least squares regression to the $u_*^2(t)$ values over the ocean, of which there is one estimate every 500 m of fetch.

An independent predictor for the advective-decay timescale that is based only on the vertical velocity fluctuations in the upstream boundary layer over land is

$$\tau_L = (L_s + c)/\sigma_w, \tag{9}$$

where L_s is the eddy length scale for the turbulence in the land-based boundary layer based on the vertical velocity spectra (section 2), σ_w is the standard deviation of the vertical velocity in the land-based boundary layer, and c is a constant that crudely compensates for influences other than decay. The formulation for τ_L is analogous to traditional theory for dissipation of turbulence variances, where the dissipation timescale increases with the characteristic length scale of the eddies and decreases with the strength of the mixing. If decay of advected turbulence dominates the sea surface momentum flux in stable offshore flow, τ_L should be related to timescale τ.

We find that the timescale τ, which represents the observed rate of decrease in the sea surface momentum flux [Eq. (8)], and the predictor timescale τ_L are indeed related (Fig. 8). That is, the spatial structure of the sea surface momentum flux depends on the characteristics of the turbulence in the upstream boundary layer over land. This implies that advection and decay processes primarily determine the air–sea momentum exchange. Using an alternate eddy length scale for the turbulence in the land-based boundary layer equal to L_s plus a constant [$c = 70$ m in Eq. (9)] in evaluating τ_L leads to a linear one-to-one relationship between τ and τ_L (plus signs in Fig. 8). One interpretation of $c > 0$ is that the turbulence is not in pure decay and that generation of turbulence over the water is not negligible. Using $c > 0$ effectively increases L_s and slows the net rate of decay.

5. Momentum budget

Horizontal advection is the largest term close to the coast (Table 2) in the equation of motion for the offshore mean wind [Eq. 7] due to acceleration (deceleration in unstable case) of the mean wind and due to the generally strong wind speeds. An increase in the low-level mean wind speed in the first several kilometers offshore is associated with an increase in the downward momentum flux with height and with mean sinking motion. Vertical

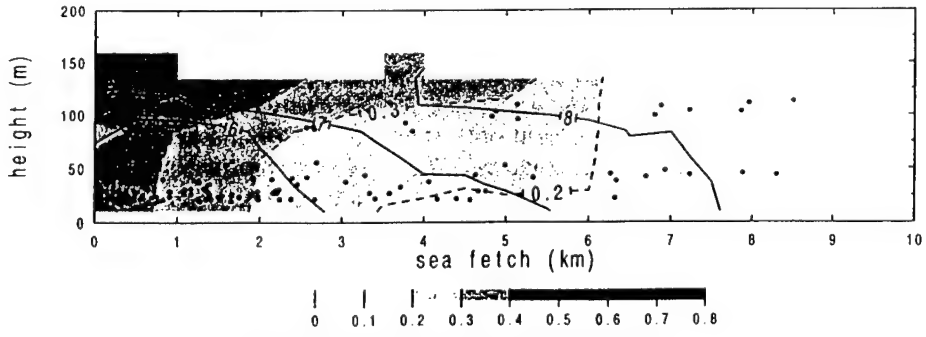

FIG. 5. Same as Fig. 3 except for case 0317.

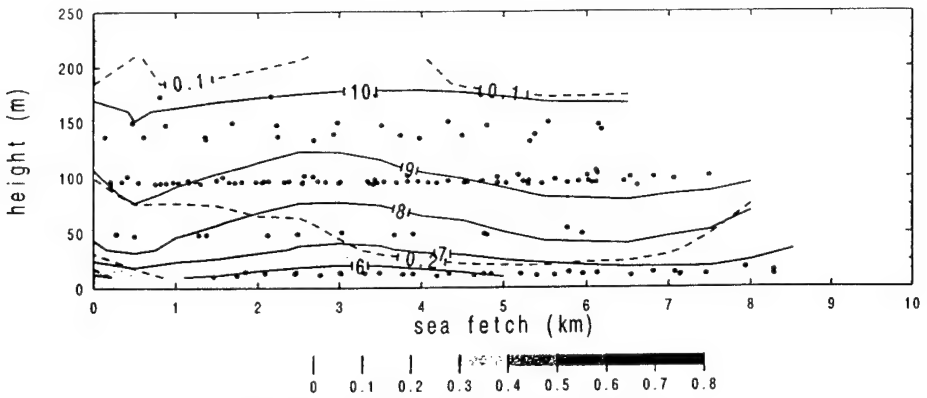

FIG. 6. Same as Fig. 3 except for case 1203a.

advection brings stronger momentum down toward the surface since the mean wind speed increases with height. The three cases with these characteristics (0318, 1114, and 0317) are stable flow of warm air over cooler water. The case with flow of cool air over warm water (1203a in Table 2) is associated with deceleration of the mean wind, a decrease in the momentum flux with height, and mean rising motion. The statistical uncertainty in the magnitude of the horizontal advection and vertical flux divergence terms is 20% or less. The remaining terms are less certain (Table 2).

The hydrostatic part of the horizontal pressure gradient due to the local horizontal temperature gradient is small compared to the residual pressure gradient (the gradient required for balance) except in the unstable case (1203a in Table 2). In this unstable case, they are approximately equal and Eq. (7) is nearly balanced. The large-scale horizontal pressure gradient from the reanalysis model (-0.49 m s^{-1} per hour) is small in this unstable case. In the three stable cases, the large-scale reanalysis pressure gradient has the same sign and approximately the same magnitude as both the vertical advection and the vertical flux divergence terms. These large-scale pressure gradients are of the correct sign to help balance local horizontal advection but significant residual remains in the budget for cases 0318 and 1114. The local momentum budget inbalance as a percentage of the horizontal advection term when using the large-scale pressure gradient is 30%, 53%, and 2% for the stable cases 0318, 1114, and 0317, respectively.

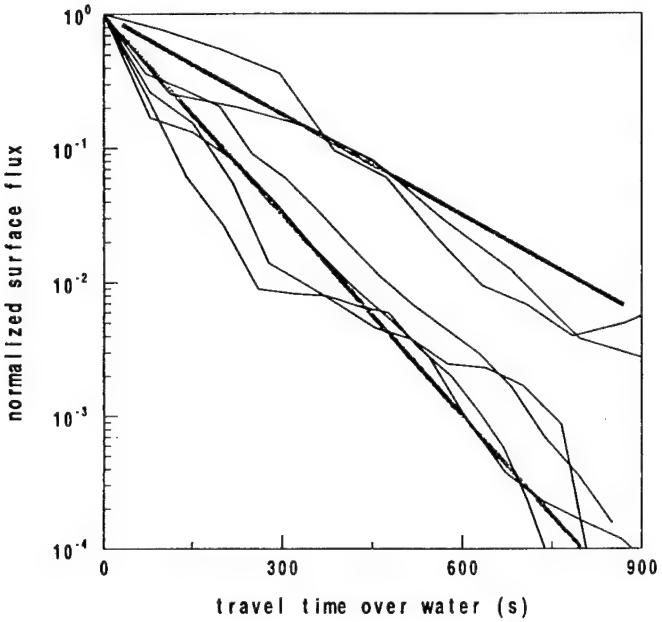

FIG. 7. Decrease in the normalized sea surface momentum flux $(u_*^2(t) - u_{*eq}^2)/(u_{*o}^2 - u_{*eq}^2)$ vs travel time over the water (t). The two heavy lines are the predicted decrease from Eq. (8) for values of the advective-decay timescale τ equal to 200 s (lower line) and 400 s (upper line).

6. Conclusions

Aircraft measurements taken during offshore flow near a barrier island on the east coast of the United States during the Shoaling Waves Experiment have been examined. For stable flow of warm air over cool water, the sea surface momentum flux decreases rapidly with increasing fetch for the first few kilometers offshore and gradually reaches equilibrium values 10 km offshore. The observed decrease in the sea surface momentum flux with travel time from the coast is predicted using a characteristic timescale of the turbulence in the upstream boundary layer over land. This suggests that, close to the coast, advection and decay of residual turbulence strongly influence the air–sea momentum exchange. In this case, similarity theory is not adequate to predict the flux due to dependence on upstream conditions.

With flow of stable warm air over cool water, the residual turbulence advected from land becomes partially detached from the sea surface leading to a momentum flux and turbulence energy maxima aloft. Contrary to the usual concept of a boundary layer, the downward momentum flux increases with height. This is due to a combination of stronger dissipation of the advected turbulence at lower levels and less travel time available

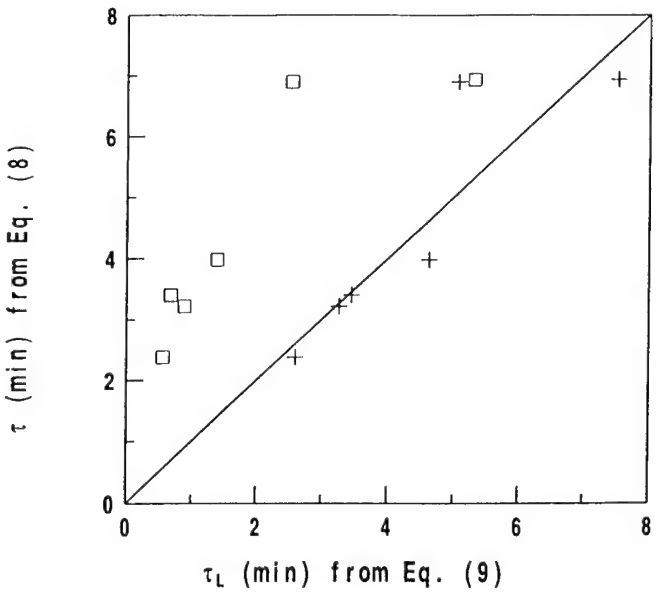

FIG. 8. Advective-decay timescale τ based on observed decrease in u_*^2 with travel time [Eq. (8)] vs τ_L calculated from characteristics of the upstream land-based boundary layer [Eq. (9) with $c = 0$] for six different case studies (squares). The plus signs show τ vs τ_L using $c = 70$ m in calculating τ_L.

for decay at higher levels due to the increase in the mean wind with height.

With flow of unstable cool air over warm water, advection and decay of residual turbulence also occur. However, the relative contribution to the total turbulence level is less due to buoyancy generation of turbulence over the ocean. Unlike the stable case, the sea surface momentum flux for unstable flows is relatively invariant with fetch or travel time. In the unstable case, the momentum flux decreases with height as in traditional boundary layers.

Estimates of the individual terms in the equation of motion for the offshore mean wind show that horizontal advection is the largest term. The vertical advection term, the vertical flux divergence term, and the horizontal pressure gradient term all act to balance horizontal advection. Acceleration (deceleration) of the mean flow in the first few kilometers offshore is associated with an increase (decrease) in the downward momentum flux with height and mean sinking (rising) motion.

Acknowledgments. We thank the NOAA LongEZ group for the field support. The useful comments of the reviewers are greatly appreciated. This work was supported by the Office of Naval Research under Grant N00014-97-1-0279.

REFERENCES

Banner, M. L., 1990: The influence of wave breaking on the pressure distribution in wind–wave interactions. *J. Fluid Mech.*, **211,** 463–495.

Crawford, T. L., and R. J. Dobosy, 1992: A sensitive fast-response probe to measure turbulence and heat flux from any airplane. *Bound.-Layer Meteor.*, **59,** 257–278.

Donelan, M. A., 1990: Air–sea interaction. *Ocean Engineering Science,* B. LeMehaute and D. M. Hanes, Eds., John Wiley and Sons, 239–292.

Fairall, C. W., E. F. Bradley, D. P. Rogers, J. B. Edson, and G. S. Young, 1996: Bulk parameterization of air–sea fluxes for Tropical Ocean-Global Atmosphere Coupled-Ocean Atmosphere Response Experiment. *J. Geophys. Res.*, **101,** 3747–3764.

Garratt, J. R., 1990: The internal boundary layer—A review. *Bound.-Layer Meteor.*, **50,** 171–203.

Geernaert, G. L., S. E. Larsen, and F. Hansen, 1987: Measurements of the wind stress, heat flux and turbulence intensity during storm conditions over the North Sea. *J. Geophys. Res.*, **92,** 127–139.

Högström, U., 1996: Review of some basic characteristics of the atmospheric surface layer. *Bound.-Layer Meteor.*, **78,** 215–246.

Horst, T. W., and J. C. Weil, 1994: How far is far enough? The fetch requirements for micrometeorological measurements of surface fluxes. *J. Atmos. Oceanic Technol.*, **11,** 1018–1025.

Howell, J. F., and L. Mahrt, 1997: Multiresolution flux decomposition. *Bound.-Layer Meteor.*, **83,** 117–137.

Kalnay, E., and Coauthors, 1996: The NCEP/NCAR 40-Year Reanalysis Project. *Bull. Amer. Meteor. Soc.*, **77,** 437–471.

Mahrt, L., D. Vickers, J. B. Edson, J. M. Wilczak, and J. Hare, 2001: Boundary-layer transitions in offshore flow. *Bound.-Layer Meteor.*, in press.

Monin, A. S., and A. M. Yaglom, 1975: *Statistical Fluid Mechanics: Mechanics of Turbulence.* MIT Press, 769 pp.

Nieuwstadt, F., and R. Brost, 1986: The decay of convective turbulence. *J. Atmos. Sci.*, **43,** 532–546.

Smedman, A.-S., M. Tjernström, and U. Högström, 1993: Analysis of the turbulence structure of a marine low-level jet. *Bound.-Layer Meteor.*, **66,** 105–126.

Sorbjan, Z., 1997: Decay of convective turbulence revisited. *Bound.-Layer Meteor.*, **82,** 501–515.

Sun, J., D. Vandemark, L. Mahrt, D. Vickers, T. L. Crawford, and C. Vogel, 2001: Momentum transfer over the coastal zone. *J. Geophys. Res.*, in press.

Vickers, D., and L. Mahrt, 1997: Quality control and flux sampling problems for tower and aircraft data. *J. Atmos. Oceanic Technol.*, **14,** 512–526.

TABLE 2. Terms in the equation of motion for different case studies in units of m s^{-1} per hour. The horizontal pressure gradient term was calculated as a residual from the equation of motion. Values in parentheses are estimates of the standard error.

Date (mmdd)	$\partial U/\partial t$	$U\partial U/\partial x$	$W\partial U/\partial z$	$\partial \overline{w'u'}/\partial z$	$\partial \overline{u'u'}/\partial x$	$\frac{1}{\rho}\partial P/\partial x$
0318	0.9 (0.4)	8.1 (0.4)	−1.6 (0.7)	−2.3 (0.4)	−0.5 (0.1)	−4.7
1114	0.7 (0.6)	13.7 (0.9)	−1.5 (0.9)	−2.4 (0.3)	−0.7 (0.2)	−9.9
0317	1.3 (0.7)	8.7 (0.3)	−3.9 (1.1)	−3.3 (0.5)	−0.6 (0.1)	−2.2
1203a	0.2 (0.6)	−8.4 (1.1)	3.3 (1.2)	1.1 (0.2)	−0.1 (0.1)	3.9

JOURNAL OF GEOPHYSICAL RESEARCH, VOL. 106, NO. D12, PAGES 12,437–12,448, JUNE 27, 2001

Momentum transfer over the coastal zone

Jielun Sun,[1,2] Douglas Vandemark,[3] Larry Mahrt,[4] Dean Vickers,[4] Timothy Crawford,[5] and Christoph Vogel[6]

Abstract. Spatial variations of surface stress over the coastal shoaling zone are studied offshore of Duck, North Carolina, by the LongEZ research aircraft, equipped to measure both atmospheric turbulence and oceanic waves. We find that the spatial variation of the friction velocity with offshore distance is much larger with offshore flow than with onshore flow. In general, the mean square slope of the short waves (wavelength shorter than 2 m) decreases with offshore distance, while the mean square slope of the long waves (wavelength longer than 2 m) increases with offshore distance. With onshore flow the friction velocity is strongly correlated with surface waves. In addition, the variation of the neutral drag coefficient is well correlated with the atmospheric bulk Richardson number. With offshore flow the observed momentum flux significantly decreases with offshore distance. Within the first few kilometer offshore, the relationship between the friction velocity and the mean square slope of the short waves and the relationship between the neutral drag coefficient and the atmospheric bulk Richardson number are obscured by the direct influence of the upstream land surface on the measured turbulence. These relationships for offshore flow agree well with those for onshore flow if the fetch is beyond the immediate influence of the land surface. The results in this study suggests that the effects of the strong turbulence advected from over the nearby land surface in offshore flow may lead to ambiguous physical interpretation of the correlation between the momentum flux and the wave state.

1. Introduction

Surface stress over the sea has been investigated over open water from ships and aircraft and over coastal water with research towers [*Geernaert and Plant*, 1990; *Weller et al.*, 1991; *Kraus and Businger*, 1994; *Mahrt et al.*, 1996]. Numerous researchers have found that the stress is greater over a young and developing wave field than over an older wave field [*Kitaigorodskii*, 1973; *Geernaert et al.*, 1987; *Donelan*, 1990; *Donelan et al.*, 1993]. Developing waves are commonly observed with atmospheric flow acceleration (changing wind direction or speed), and fetch-limited offshore flow [*Geernaert et al.*, 1987], while the older wave field is closer in equilibrium with the wind field. Young developing waves (small wave age) are dominated by the growth of high-frequency capillary waves and small gravity waves that ride on the top of long gravity waves, travel slower than the wind, and thus lead to high surface stress [*Donelan*, 1982; *Geernaert et al.*, 1986].

Fully developed waves (larger wave age) move with a phase speed close to the wind speed and are associated with relatively low surface stress. Analysis of RASEX (RisøAir-Sea Experiment) data indicated that most of the variation of the drag coefficient could be explained in terms of wave age although self-correlation through the friction velocity accounted for much of this explained variance, and the broadness of the wave spectra explained additional variance [*Vickers and Mahrt*, 1997a]. The influence of directional differences of the wind, wind stress, and surface waves on the open ocean has been studied by *Geernaert* [1988a], *Geernaert et al.* [1993], and *Rieder et al.* [1994].

Interactions between the stress and the sea surface immediately off coastlines are not fully understood [*Mahrt et al.*, 1996, 1998; *Mahrt*, 1999]. In the coastal zone, large stress is expected with shoaling processes and wave breaking as swell propagate into shallow water [*Smith*, 1980; *Freilich and Guza*, 1984]. Therefore spatial variations of turbulent fluxes over the coastal

[1]National Center for Atmospheric Research, Boulder, Colorado.

[2]Also at Program in Atmospheric and Oceanic Sciences, University of Colorado, Boulder, Colorado.

[3]NASA Goddard Space Flight Center, Wallops Island, Virginia.

[4]College of Oceanic and Atmospheric Sciences, Oregon State University, Corvallis.

[5]NOAA Field Research Division, Idaho Falls, Idaho.

[6]NOAA Atmospheric Turbulence and Diffusion Division, Oak Ridge, Tennessee.

Paper number 2000JD900696.
0148-0227/01/2000JD900696$09.00

zone are expected to be large [*Crawford et al.*, 1993; *Mahrt*, 1999].

For the first time, the spatial variation of the air-sea interaction in the shoaling zone is studied with both atmospheric and surface-wave observations on board the research aircraft, LongEZ. The observed atmospheric and oceanic data used in this study are described in section 2. Methods of data analysis are explained in section 3. The momentum transfer between the atmosphere and the sea surface is investigated for onshore and offshore flows in section 4. A summary of the study is given in section 5.

2. Observations

Two experiments were conducted off the coast of Duck, North Carolina, one from October 26 to November 12, 1997, and the other one from March 1 to 17, 1999. The LongEZ aircraft (Figure 1) was equipped to measure all three wind components, air temperature, and atmospheric pressure at 50 samples per second, and surface radiation temperature (Everest Interscience Inc., 4000.4GL infrared radiometer) at 1 sample per second [*Crescenti et al.*, 1999]. The high sampling rate and the fast-response instrumentation of the air-motion measurements enables us to calculate atmospheric turbulent fluxes using eddy-correlation methods. The aircraft typically flies at 55 ms^{-1} at 15 m above the sea surface.

Three laser altimeters (Riegl model LD90-3 VHS) were mounted in a triangle with triangle legs of 0.93 m, 0.94 m, and 0.94 m to simultaneously measure sea surface wave heights [*Vandemark et al.*, 2000]. The laser range accuracy and precision are better than 2 cm. The minimum surface wave length derived from the laser altimeters is about 2 m. A downward looking Ka-band continuous wave (CW) radar scatterometer was also on board, and its 1 m diameter field of view overlays the field of view of the three laser altimeters [*Vandemark et al.*, 2000]. In addition to the onaboard downward looking scatterometer and the three laser altimeters, a Datawell Directional Waverider buoy, moored at about 20 m depth and 5 km offshore, was operated by Thomas Herbers's group at the Naval Postgraduate School during the 1997 experiment.

There were 16 aircraft flights conducted in the 2 week experiment in November, 1997, and 23 aircraft flights in the 3 week experiment in March 1999. Repeated runs for each flight track were designed to ensure adequate flux sampling. Two main flight patterns were flown to study spatial variations of atmospheric turbulence and surface waves as functions of offshore distance: one consists of tracks parallel to the coastline at various offshore distances; and one consists of many repeated runs along a track perpendicular to the coastline (Figure 2). For the parallel track flight, there are typically two to four passes along each track. For the perpendicular track flight there are typically eight passes. During both experiments the tracks parallel to the coastline are about 20 km long. The track perpendicular to the coastline is about 10 km long and is extended to 90 km offshore for some flights. In this study we mainly focus on flights with both the atmospheric turbulence and the wave data available. On the basis of these criteria, four parallel flights (Flights 5, 12, 14, and 15) and two perpendicular flights (Flights 3 and 16) from the 1997 experiment and three parallel flights (Flights 5, 9, and 10) from the 1999 experiment are selected (Table 1). Among these nine flights, the radar data are available for all the flights except Flight 12 from the 1997 experiment. The wind was onshore for Flights 14 and 15 of the 1997 experiment, offshore for Flights 3, 5, 12 of the 1997 experiment, and Flights 5 and 9 of the 1999 experiment, and almost parallel to the coastline for Flights 16 of the 1997 experiment and Flight 10 of the 1999 experiment (Table 1).

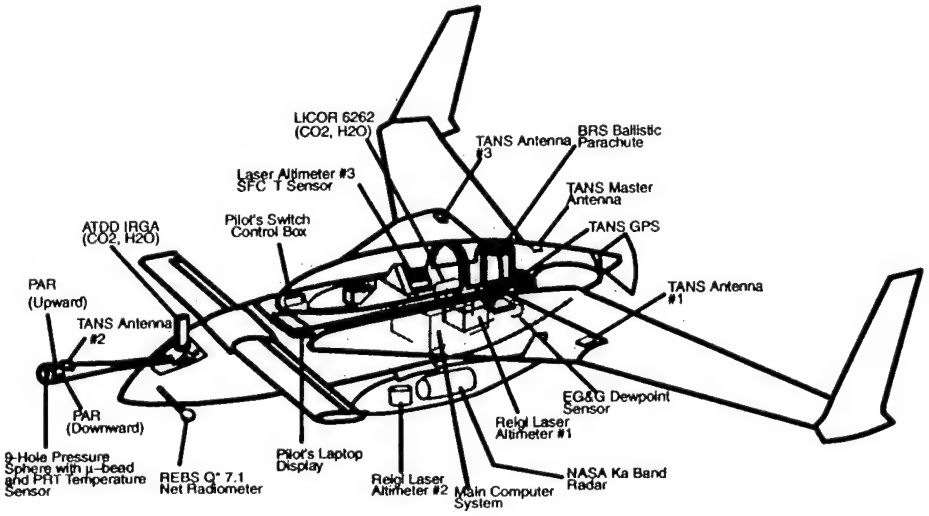

Figure 1. Schematic diagram of the equipment on the NOAA LongEZ.

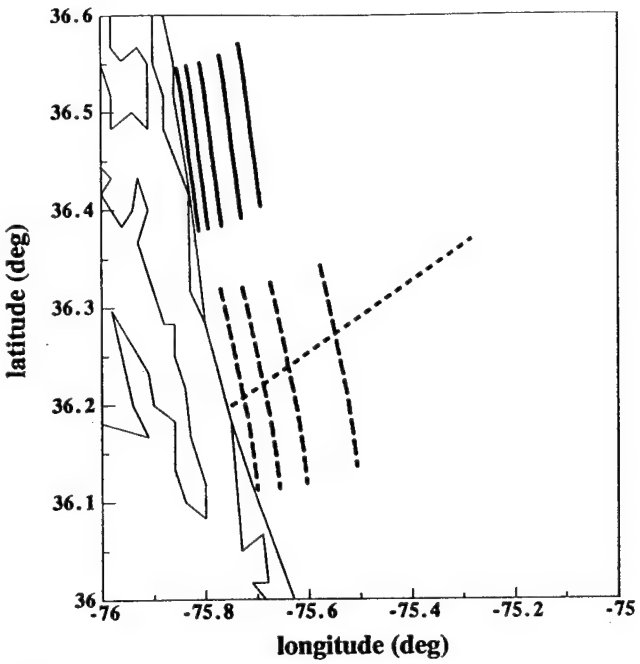

Figure 2. Schematic diagram of flight tracks. The solid lines are the parallel tracks in the 1999 experiment. The dashed lines are the parallel tracks and the perpendicular track in the 1997 experiment.

3. Data Processing

The aircraft position and velocity are obtained by combining differential GPS (global positioning system) with the information from the accelerometers, recorded at 10 samples per second and 50 samples per second, respectively. The aircraft platform attitude is obtained by combining TANS (Trimble Advanced Navigation System) GPS attitude, recorded at 10 samples per second, with the information from the accelerometers [*Crawford and Dobosy*, 1992].

All the aircraft data used for the analysis in this paper were quality-controlled following *Vickers and Mahrt* [1997b]. After eliminating records with apparent instrumentation problems, the turbulent fluxes are calculated by averaging products of the perturbations from nonoverlapping windows of 1 km width. The qualitative results of this study, such as the general character of the spatial variation of turbulent fluxes, were not sensitive to the averaging window size. Assuming spatial homogeneity along each flight track, the random flux error (f_{err}) for the momentum transfer is normally less than 8% for the repeated flight tracks parallel to the coastline. Here the random flux error f_{err} is calculated as

$$f_{err} = \frac{\sigma_f}{\sqrt{N}}, \tag{1}$$

where σ_f is the standard deviation of the flux for a given flight track, and N is the total number of 1 km flux values. For the parallel flight track, N is typically between 40 and 80 for each flight track.

The nadir-looking radar backscatter is measured as the normalized radar cross section (NRCS), which is inversely correlated with the mean square slope (mss) of these surface waves [*Barrick*, 1974; *Vandemark et al.*, 1997],

$$\mathrm{mss} = C \times 10^{(-\mathrm{NRCS}/10)}, \tag{2}$$

where the Fresnel reflection coefficient C for the *Ka*-band (36 GHz) radar is 0.52. At a 15 m flight level, the instantaneous backscatter encompasses surface waves with horizontal length scales of 1 m down to scales of the order of the 8 mm radar radiation wavelength; that is, the instantaneous radar backscatter signal strength depends on surface waves with wavelengths between 1 m and 25 cm. The total mean square slope estimate is derived from the ensemble of the NRCS over the two-scale process of sweeping this 1 m field of view along varying underlying waves as the aircraft flies over a given flight segment. Theoretical prediction and measurements indicate that surface wind stress and nadir-looking radar backscatter are related to the integrated wave slope [*Brown*, 1979; *Kitaigorodskii*, 1973], particularly in the capillary-gravity-wave range [*Wu*, 1972]. A typical averaging segment is 3 km, and the computed random error for a given NRCS estimate is of the order of 2% [*Vandemark et al.*, 2000].

The mean square slope of the surface waves for wavelengths longer than 2 m can be calculated from the three simultaneous laser altimeter measurements corrected for the aircraft motion [*Vandemark et al.*, 2000].

Table 1. Flight Information

Case	Flight	Date	LT	Radar /Laser	Flow Versus Coast	Flight Track	Wind Direction (deg)	Wind Speed (m/s)
1	F3	Nov. 2, 1997	1153	yes	offshore	perpendicular	233.8	7.8
2	F5	Nov. 3, 1997	1326	yes	offshore	parallel	195.6	7.0
3	F12	Nov. 9, 1997	1301	no	offshore	parallel	286.6	8.2
4	F14	Nov. 10, 1997	1119	yes	onshore	parallel	32.2	3.6
5	F15	Nov. 10, 1997	1347	yes	onshore	parallel	73.8	2.6
6	F16	Nov. 11, 1997	0734	yes	parallel	perpendicular	356.3	5.8
7	F5	Mar. 4, 1999	1052	yes	offshore	parallel	272.4	11.2
8	F9	Mar. 6, 1999	1006	yes	offshore	parallel	189.5	7.7
9	F10	Mar. 7, 1999	1028	yes	parallel	parallel	339.4	13.3

For simultaneous measurements from three laser altimeters the unit vector normal to the wave surface measured by the three lasers, $\vec{S}$, is

$$\vec{S} = \frac{(\vec{L}_3 - \vec{L}_2) \times (\vec{L}_2 - \vec{L}_1)}{|\vec{L}_3 - \vec{L}_2| \cdot |\vec{L}_2 - \vec{L}_1|}. \quad (3)$$

Here $\vec{L}_1 = (x_1, y_1, z_1)$, $\vec{L}_2 = (x_2, y_2, z_2)$, and $\vec{L}_3 = (x_3, y_3, z_3)$ represent the locations of the intersections between the three laser beams and the sea surface. The distances, z_1, z_2, and z_3, are measured from the three laser altimeters with the aircraft motion removed, and the coordinates x_i and y_i $(i = 1, 2, 3)$ are the location of the three lasers relative to the aircraft gravity center on the horizontal aircraft plane . The sea surface slope s is then

$$s = \tan(\theta), \quad (4)$$

where

$$\cos(\theta) = \vec{S} \cdot \vec{k}. \quad (5)$$

Here $\vec{k}$ is the upward unit vector, and θ is the angle between the wave surface and the flat sea surface.

The total mean square slope for the surface waves measured using three lasers, mss_l, can be readily estimated as

$$\text{mss}_l = \frac{1}{M} \sum_{i=1}^{M} s_i^2, \quad (6)$$

where s_i is the slope s at each time i, and M is the total number of the laser range measurements used for estimating mss_l. In this study, M is 3000 for a 3 km segment. Several calibration flights with substantial aircraft roll and pitch maneuvers were performed over smooth water on the inland sound to asses the fidelity of the aircraft motion removal on the derived sea surface elevation and wave slope data. For these cases the mss_l value was typically less than 0.002 with along-track variations of less than 10%. On the basis of these tests we conservatively estimate the maximum relative error for open-ocean mss_l to be 5%.

The mean square slope of short waves (mss_s) for wavelengths shorter than 2 m can be estimated by combining the mean square slope of the integrated surface waves from the radar scatterometer (mss) for wavelengths longer than 2.5 cm and the mean square slope of the surface waves from the laser altimeters (mss_l) for the wavelengths longer than 2 m,

$$\text{mss}_s \approx \text{mss} - \text{mss}_l; \quad (7)$$

that is, the mean square slope of the short waves is estimated as the difference between the mean square slope of "total" wave field estimated from the radar scatterometer and the mean square slope of the long waves estimated from the laser altimeters. Therefore mss_s is derived from the measurements of two different instruments.

Assuming the homogeneity of each flight track, all the observed variables, including the turbulent fluxes and the mean square slope of the surface waves: mss_s, mss_l, and mss are averaged from repeated 20 km long passes over each flight track for the tracks parallel to the coastline to study the spatial variation of these variables as a function of offshore distance. The fluxes and the mean square slope of the surface waves along the flight tracks perpendicular to the coastline are fitted as a function of offshore distance based on repeated passes.

One-dimensional wave height spectra for those waves propagating along the flight direction can be derived from the spatial wave elevation series collected from any of the three laser altimeters aboard the LongEZ after adjusting for aircraft motion. For waves traveling perpendicular to the aircraft heading, some a priori knowledge of their direction is required when using measurements from only one laser altimeter. The wave measurement from the altimeter is analogous to wave measurements from wave rider buoys, except wave rider buoys measure wave heights as functions of time, while laser altimeters measure wave heights as functions of horizontal distance.

The atmospheric stability in this study is expressed in terms of the bulk Richardson number (R_i),

$$R_i = -\frac{g\ \Delta\theta\ z}{\theta_0\ U^2}, \quad (8)$$

where

$$\Delta\theta = T_s - T_a. \quad (9)$$

In equations (8) and (9), g is the gravity constant, z is the observation height, θ_0 is the reference potential temperature, set to be 285.15 K, U is the wind speed, and T_s and T_a are the sea surface skin temperature measured by the infrared radiometer and the air temperature measured from the LongEZ, respectively.

4. Spatial Variations of Stress in the Shoaling Zone

Surface stress ($\vec{\tau}$) between the atmosphere and the sea surface over open water can be estimated as

$$\vec{\tau} = \rho(\overline{w'u'}\ \vec{i} + \overline{w'v'}\ \vec{j}), \quad (10)$$

where ρ is the air density; u', v', and w' are the wind speed fluctuations in the north-south $\vec{i}$, east-west, $\vec{j}$, and vertical, $\vec{k}$, directions, respectively. In this study, the mean value is defined as an unweighted window average over 1 km. The strength of the stress will be expressed in terms of the friction velocity (u_*), defined as

$$\tau = \rho u_*^2. \quad (11)$$

On the basis of Monin-Obukhov similarity theory the friction velocity depends on wind speed, atmospheric stability, and sea surface roughness; that is,

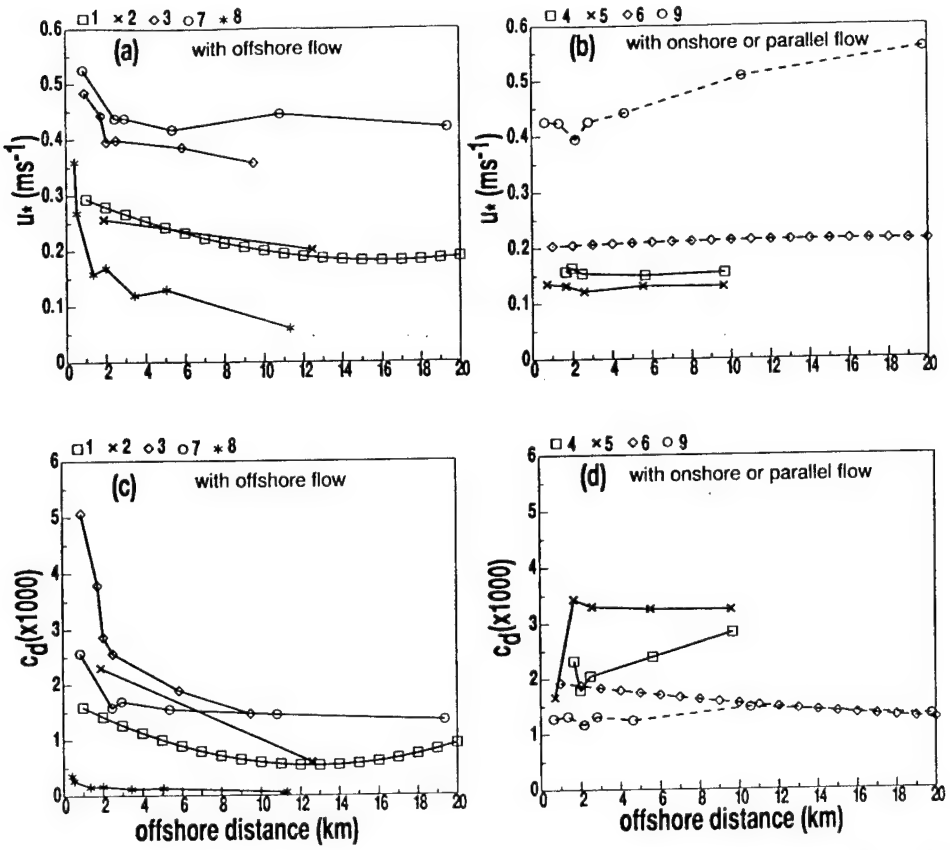

Figure 3. Friction velocity (u_*) (a, b) and drag coefficient (C_d) (c, d) as functions of offshore distance for onshore flow (b, d), and offshore flow (a, c) cases. Each individual symbol represents composited results from one flight. The numbers at the top of each panel represent the case number listed in Table 1. The dashed lines in Figures 3b and 3d represent the cases where the flow is almost parallel to the coast.

$$u_* = C_d^{1/2} U, \tag{12}$$

where

$$C_d^{1/2} = \frac{\kappa}{\ln(z/z_0) - \Psi_m(z/L)}. \tag{13}$$

Here C_d is the drag coefficient, U is the mean wind speed, z_0 is the aerodynamic roughness length, κ is the von Karman constant, and Ψ_m is the stability function for momentum expressed in terms of z/L, where $L = -\bar{\theta}_v u_*^3/(\kappa g \overline{w'\theta_v'}|_s)$ is the Obukhov length, and θ_v and $\overline{w'\theta_v'}|_s$ are the virtual potential temperature and the buoyancy flux at the surface, respectively. In this study, the *Paulson* [1970] and *Dyer* [1974] stability functions are used for unstable and stable regimes, respectively. The ocean current is assumed to be much smaller than the wind speed in equation (12). Removing the stability influence in equation (13), the neutral drag coefficient can be expressed as

$$C_{d0}^{1/2} = \frac{\kappa}{\ln(z/z_0)}. \tag{14}$$

If z is constant, the neutral drag coefficient is monotonically related to the aerodynamic roughness length z_0, which is related to the physical roughness of the underlying surface if the stress is generated by the interaction between the airflow and the underlying wave surface. Using the aircraft observational data, the neutral drag coefficient can be calculated using equations (10)-(14).

4.1. Spatial Variation of Stress As a Function of Offshore Distance

On the basis of the LongEZ data described in section 2 the surface friction velocity significantly decreases with offshore distance within the first several kilometers off the coast in offshore flow (Figure 3a), while the corresponding spatial variation of the friction velocity for onshore flow is small (Figure 3b). The difference in the spatial variation of the surface stress between the onshore and the offshore flow cases is also clearly demonstrated in terms of the drag coefficient (Figure 3c and 3d), in which case the dependence of the stress on the wind speed has been removed (equation (13)). The drag coefficient systematically decreases with offshore distance in the offshore flow cases but not in the onshore flow cases.

For scalar quantities the rapid change of the observed flux with fetch, immediately downstream from

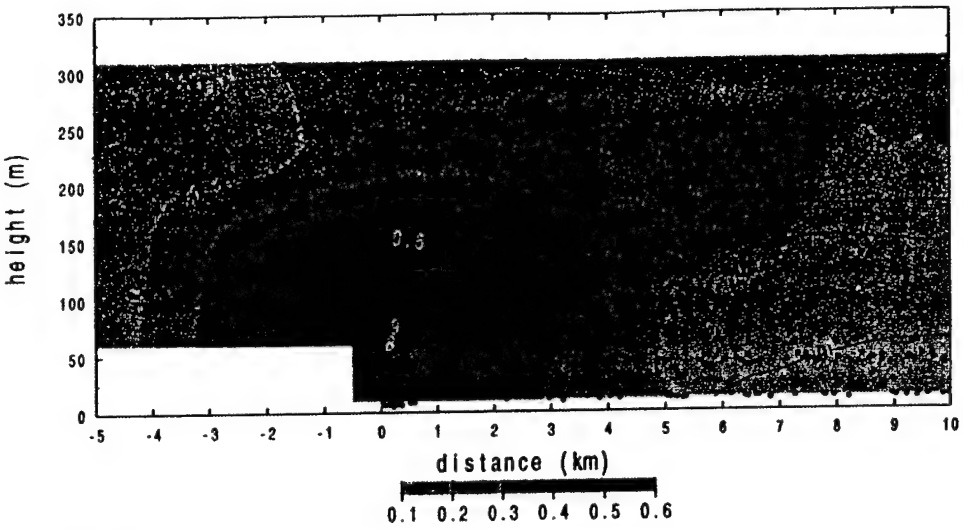

Figure 4. Vertical cross section of the friction velocity (shaded with dashed contours) and the wind speed (solid contours) for November 14, 1999. Here zero distance represents the Atlantic coastline of Outer Banks. The Outer Banks are about 4.2 km wide in this cross section. The negative distance represents the distance west of the Atlantic coastline of the Outer Banks. The plot is based on aircraft measurements of the friction velocity calculated from 1 km segments. The 1 km segments used for this plot are indicated by the dots. The wind was offshore from the southwest. The technique for construction of the distance-height crosssection is described by *Vickers et al.* [2001].

the coast, can be viewed in terms of footprint theory. For momentum, stress and turbulence energy the footprint theory is not strictly valid because footprint theory is formally based on the advective-diffusion equation, and the role of pressure fluctuations and viscous decay are not included. We will continue to use the term "footprint" in a more descriptive context as the upstream surface region, which contributes to the momentum flux at the observation level.

With this concept the flux measured at the aircraft level contains contributions from both the sea and the upstream land surface. The contribution of the upstream land surface decreases with fetch. According to *Horst and Weil* [1994], 90% of the turbulent scalar flux measured at the height of 10 m typically originates from a footprint extending 1-2 km upstream although the footprint varies with atmospheric stability and wind speed. The vertical cross section of the momentum transfer extended to the inland sound (Figure 4) indeed shows that the rough unstable land surface between the inland sound, and the Atlantic Ocean plays an important role on the observed momentum transfer immediately off the Atlantic coastline. Therefore the true interaction between the turbulent air and the sea surface is obscured by the direct influence of the upstream land surface on the measured stress.

4.2. Spatial Variation of Surface Waves

As momentum is transferred from the atmospheric flow to the ocean by the atmospheric turbulence, surface wind waves are generated. In general, the mean square slope of the short waves (mss_s) decreases with offshore distance for both onshore and offshore flow cases. The mean square slope of the long waves (mss_l) increases with offshore distance when the wind is offshore (Figure 5).

When the flow is onshore, mss_l generally increases with offshore distance, except when the offshore distance is less than 2 km, where mss_l increases toward the coast apparently due to shoaling (Figure 5e). Such shoaling increases mss_s as well as mss_l. A similar shoaling effect was also observed by *Anctil and Donelan* [1996]. The exception for case 9 in Figure 5d is most likely due to the increase of the wind speed with the offshore distance (section 4.3).

An example of one-dimensional spectra on November 1997 (case 1 in Table 1) when the LongEZ flew perpendicular to the coastline is analyzed in this study to assess the impact of the longer waves (swell and wind-driven surface waves) on the mean square slope of surface waves in offshore flow. For the present example we broke the flight data into 2 km data segments along the flight track. Each 2 km segment contains approximately 2000 data points. A continuous Morlet wavelet transform [*Torrence and Compo*, 1998] was performed on each data segment to produce a wave-height density spectrum at each offshore distance.

On the basis of the nearby wave rider buoy data, the wind-driven sea surface waves propagated toward the northeast, and the swell traveled to the northwest (300°) with a period of 9 s. The existence of swell and wind-driven waves are evident in Figure 6a, where the

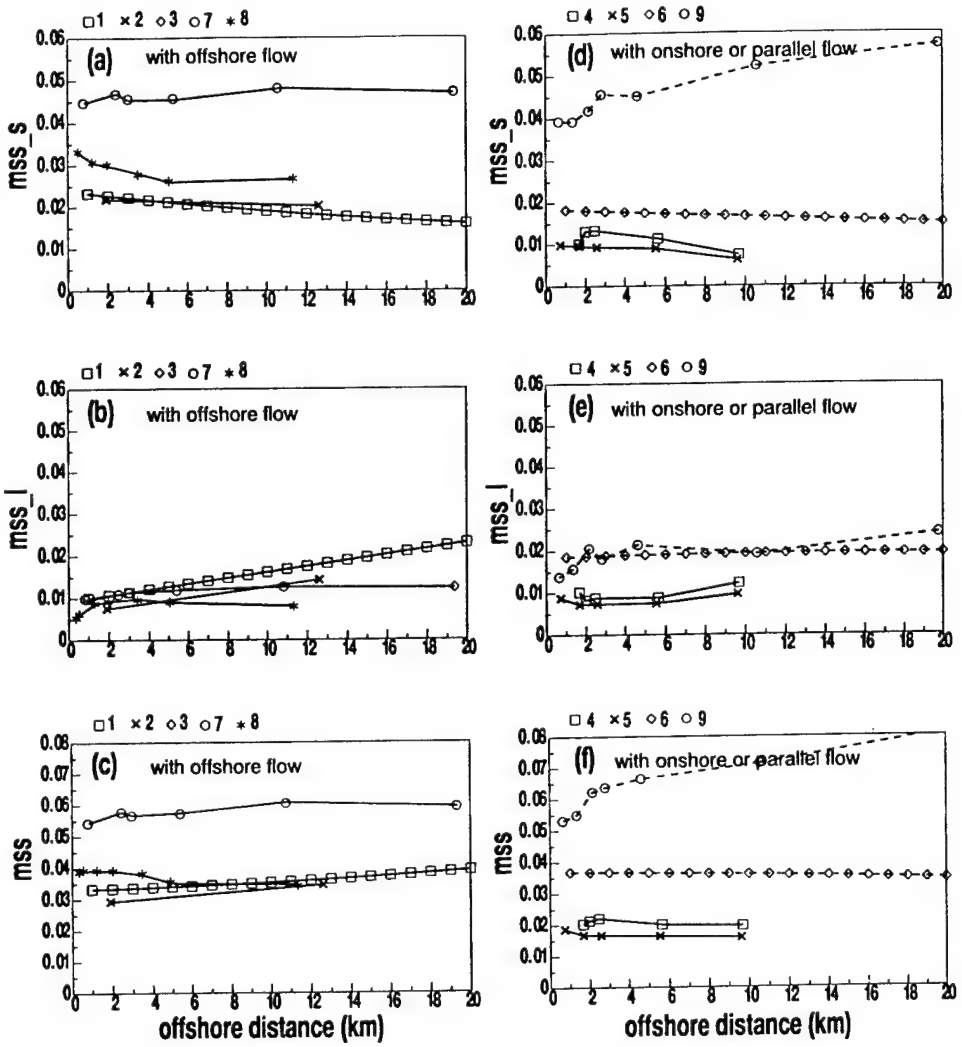

Figure 5. Mean square slopes of short surface waves (less than 2 m) (a, d), long surface waves (longer than 2 m) (b, e), and the sum of the short and long surface waves (c, f) observed by the radar and the laser altimeters as functions of the offshore distance for the onshore (d, e, f) and offshore (a, b, c) flows. The dashed lines represent the case in which the flow is almost parallel to the coastline.

derived swell wave number accords with the 9 s period swell measured by the nearby buoy. The difference between the wave spectra at 2 km and 10 km offshore in Figure 6a shows that the peak wave number of the wind-driven waves decreases with increasing offshore distance, and the amplitude of the wind-driven waves increases with increasing offshore distance as the aircraft flew nearly along the direction of the wind-driven wave propagation (Figure 6b). This spatial variation of the wind-driven surface wave is consistent with the observations from *Hasselmann et al.* [1973]. In comparison, both the wave number and the energy of the swell remained invariant (Figure 6a and 6b). Therefore the increase of the significant wave height with offshore distance is due to the increased energy of the growing wind-driven surface waves in the presence of the incoming swell (Figure 6c). Here the significant wave height is calculated as 4 times the root-mean-square wave height. The invariant swell height of about 1 m can be estimated from Figure 6c near the coastline, where the wind-driven surface wave height is negligible. These results imply that the increase of mss_l with offshore distance is closely related to the increasing wind-driven wave energy with offshore distance and the shift of the wind-driven waves to larger wavelengths.

4.3. Relationship Between Wind Stress and Sea Surface Roughness

For the offshore flow case, the large mean square slope of the short waves close to the coast is related to the young waves generated by the turbulent air as the sea surface responds to the atmospheric momentum flux. As these waves propagate offshore, the new wind-driven short waves transfer the energy to longer waves due to wave-wave interaction, as inferred in section 4.2. There is no sharp decrease of the mean square slope of short

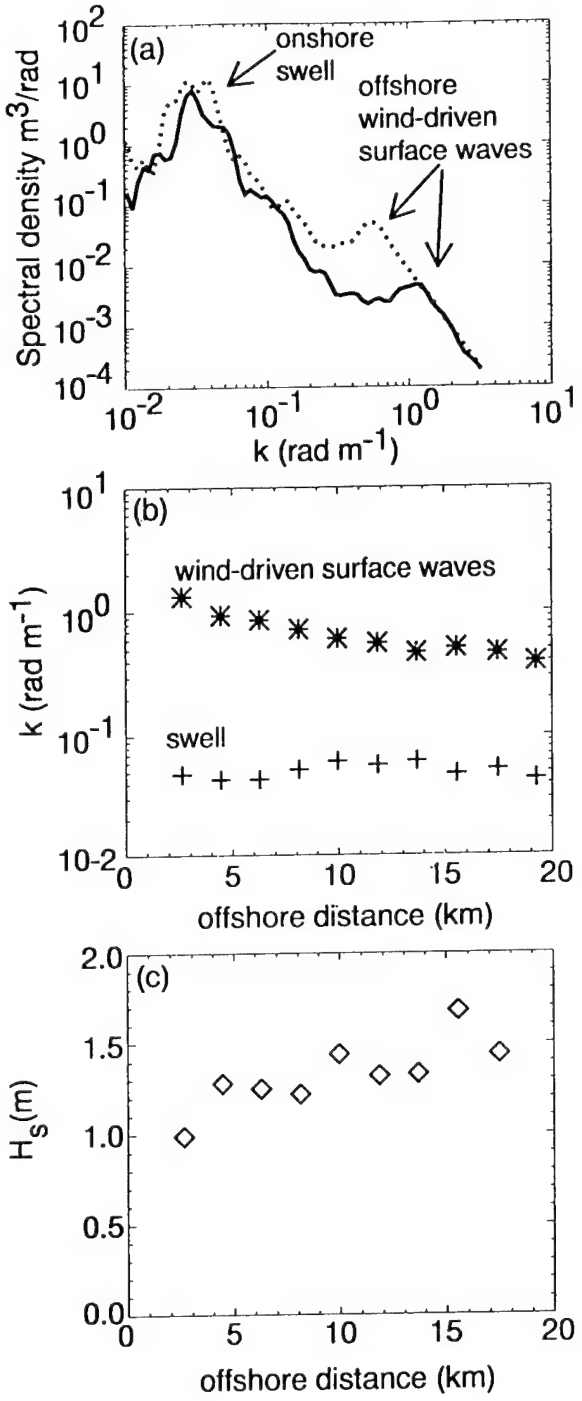

Figure 6. Wave analysis from a laser altimeter. (a) Wave height density spectra as functions of wave number at 2 km (solid line) and 10 km (dotted line) offshore. (b) The spectral peak wave numbers of the incoming swell (pluses) and the wind-driven waves (asterisks) as functions of offshore distance. Here the peak wave number of the swell is adjusted to account for the 60° angle between the swell propagation direction and the aircraft heading. (c) Significant wave heights as functions of offshore distances.

and long waves (Figure 5) for the first several kilometers offshore, in contrast to the sharp decrease of the friction velocity with the offshore flow (Figure 3). Since the observed momentum flux includes the influence of the upstream land, while the mean square slope of waves represents the sea surface state right under the observational point, the footprint of these two quantities is mismatched. The mismatch of the footprint is not very important if the spatial variation of the surface does not vary dramatically, as in onshore flow. *Nordeng* [1991] indicates that surface waves do not generate significant stress when the waves are very young, implying that the large momentum flux observed right off the coastline cannot be attributed completely to young waves. Because the footprint of the momentum flux increases with increasing observation height, the downward momentum flux at higher levels includes the land surface and is therefore larger compared to the momentum flux near the surface (Figure 4). This resulting vertical convergence of the downward momentum flux accelerates the offshore flow (Figure 7), which is also observed by *Smedman et al.* [1995].

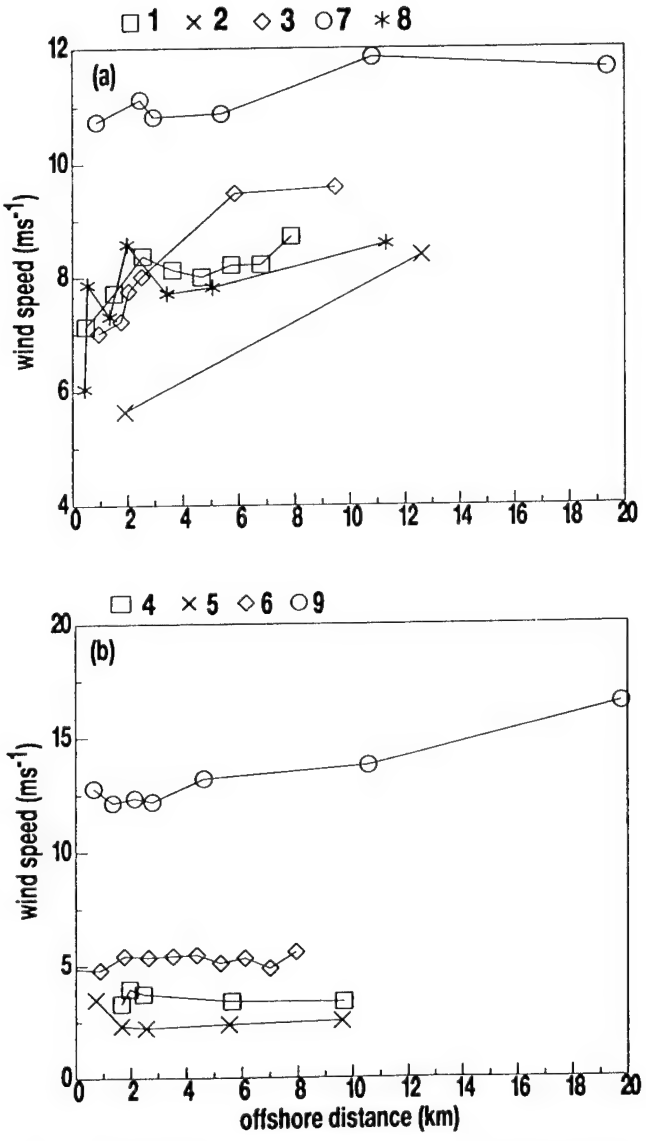

Figure 7. Wind speed as a function of offshore distance for offshore flow (a) and onshore/parallel flow (b).

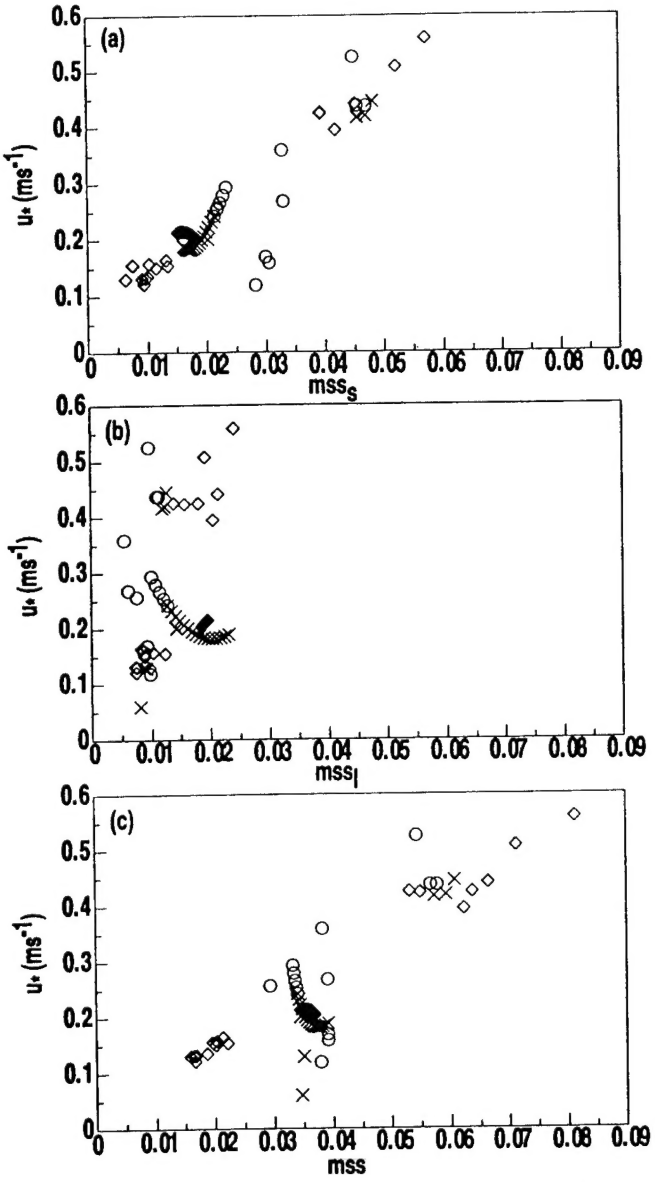

Figure 8. Relationship between the friction velocity and the mean square slope of (a) short surface waves (less than 2 m), (b) long (longer than 2 m) surface waves, and (c) the sum of the short and long surface waves observed by the radar and the laser altimeters for the onshore (diamonds) and offshore (circles and crosses are for off-distance less and greater than 5 km, respectively) flows.

With onshore flow the friction velocity and the mean square slope of the short waves are closely correlated (Figure 8), consistent with previous observations [*Cox and Munk*, 1954; *Brown et al.* 1981; *Vandemark et al.*, 1997, 1999]. For offshore flow the friction velocity is not well correlated with the mean square slope of the short waves within 5 km of the coast. Farther offshore, the relationship between the friction velocity and the mean square slope of the short waves agrees reasonably well with the relationship for the onshore flow (Figure 8).

For offshore flow and beyond 5 km offshore, the correlation between the friction velocity and mss_l is not so good as the correlation between the friction velocity and the mss_s and not so good as the correlation between the friction velocity and the mss_l for the onshore flow case. *Vickers and Mahrt* [1997a] find that the wave spectra are broader for the offshore flow than for the onshore flow. As discussed in section 4.2, our example case shows that the energy of the waves increases with offshore distance, and the peak of the wave spectra progressively shifts toward lower frequencies as the fetch increases. These long waves may result from interactions between waves that are generated upstream. These long waves can travel fast and may not be fully coupled with the surface stress. In contrast, the close correlation between the friction velocity and the mss_s in offshore flow for more than 5 km from shore indicates that the short waves are in equilibrium with the surface wind forcing.

4.4. Influence of the Atmospheric Stability on the Wind Stress

The surface roughness of the ocean ripples (mainly the capillary waves) is found to increase with the atmospheric instability [*Keller et al.*, 1985; *Hwang and Shemdin*, 1988; *Wu*, 1991]. The enhanced turbulence under unstable conditions leads to greater sea surface ripples and sea surface roughness, in contrast to stability-independent roughness lengths over land surfaces [*Sun*, 1999].

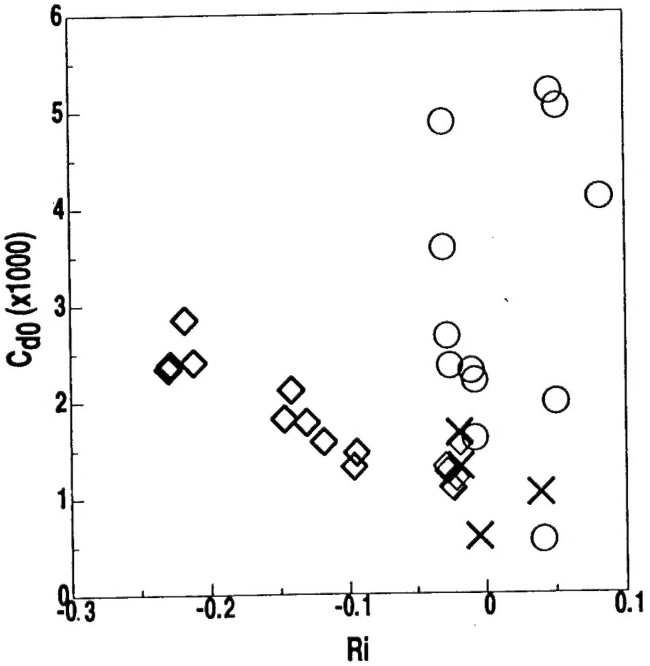

Figure 9. Neutral drag coefficient (C_{d0}) as a function of the bulk Richardson number (R_i) for both onshore (diamonds) and offshore flows (circles). The crosses represent the situation where the wind is offshore, but the offshore distance is larger than 5 km.

Figure 9 shows that the neutral drag coefficient does increase with atmospheric instability systematically for the onshore case where the downward momentum transfer is completely associated with the interaction between the atmosphere and the oceanic waves. This stability dependence of the neutral drag coefficient was also observed by *Plant et al.* [1998]. They suggested that the surface roughness increases in unstable conditions where the downward transfer of momentum to the wave surface is more efficient.

For offshore flow the neutral drag coefficient close to the coast is inevitably affected by the upstream land surface since the fluxes at the aircraft level are affected by the upstream land surface. However, the bulk Richardson number is the bulk parameter based on the mean variables over the sea surface alone. Therefore the neutral drag coefficient near the coast in offshore flow is not well correlated with the bulk Richardson number. As the footprint of the momentum flux becomes occupied completely by the sea surface when the offshore distance is larger than 5 km, the correlation between the neutral drag coefficient and the bulk Richardson number agrees reasonably well with the correlation for the onshore flow cases (Figure 9). The relationship between the neutral drag coefficient and the atmospheric stability for the onshore flow and longer fetch offshore flow implies that the spatial variation of the atmospheric stability may also play an important role in the spatial variation of the sea surface roughness.

4.5. Discussion

Geernaert [1988b] summarized seven regression formulas for the neutral drag coefficient as a function of wind speed. He found that the neutral drag coefficient was much larger over shallow water than over open water. The large neutral drag coefficient over shallow water cannot be explained entirely by the fetch-dependent sea state, therefore shoaling effects were suggested as a possible explanation. As indicated in this study, the large momentum flux observed in the coastal area with offshore flow is very likely influenced by the advection of the large momentum flux from the land surface. Therefore the advection from the land surface may explain part of the discrepancy between the observed and the modeled, wave-dependent neutral drag coefficient in the *Geernaert* [1988b] work.

Traditionally, the drag coefficient in the coastal zone is studied in terms of fetch and wave age. The wave age is designed to characterize the movement of the wind relative to surface wave motion, and in one version of the wave age is defined as the ratio of the phase speed of the most significant wave relative to the wind speed. When the wave phase speed is much slower than the wind speed (small wave age), strong atmospheric flow relative to the waves induces large drag at the sea surface. When the wave phase speed is comparable to the wind speed, the surface stress between the atmospheric motion and the moving surface waves is small [*Al-Zanaidi and Hui*, 1984]. However, the interaction between the wind and the surface waves other than the significant wave may also contribute to the surface stress when the wind-wave spectra have a wide band structure, especially when the wind generates waves on the top of the existing long waves [*Donelan et al.*, 1993; *Vickers and Mahrt*, 1999].

Alternatively, the wave age is computed as the ratio between the phase speed of the significant wave and the friction velocity [*Geernaert et al.*, 1987; *Donelan et al.*, 1993] with the implied assumption that the footprint of the turbulent fluxes is completely over the sea surface. As demonstrated in this study, the stress over the coastal water can be influenced by the strong turbulence advected from land. The large momentum flux with the offshore flow would lead to a small value of the wave age (defined with the friction velocity instead of wind speed). The wave age calculated using the observed friction velocity close to the coast would not represent the true wave state until farther offshore when the measured stress is influenced only by the sea surface.

Fetch-dependent studies of the momentum transfer in the literature may have unknowingly captured the spatial variation of the footprint of the observed flux over the land surface. Using the footprint theory as guidance, the measured flux downstream from the land surface not only depends on the distance from the coast but also on the measurement height and upstream spatial variation of the atmospheric stability.

5. Summary

The spatial variation of the interaction between the atmosphere and the sea surface in the coastal zone is studied using simultaneous measurements of the atmospheric turbulence and the sea surface from the LongEZ research aircraft. In the coastal zone the spatial variation of the surface stress and the correlation between the surface stress and the sea surface roughness are distinctly different between the onshore and the offshore flows.

For onshore-flow the friction velocity is well correlated with the mean square slope of short surface waves with wavelengths shorter than 2 m, and with the mean square slope of long surface waves with wavelengths larger than 2 m. The mean square slopes of the short and long surface waves are derived from simultaneous measurements from the downward looking *Ka*-band radar scatterometer and the three laser altimeters onboard the aircraft. The neutral drag coefficient is well correlated with the atmospheric bulk Richardson number, confirming expected interactions between the sea surface waves and the turbulent air fluctuations.

However, for the offshore flow cases, the stress decreases rapidly with offshore distance for the first several kilometers. This sharp decrease in the momentum flux is most likely due to the decreasing influence of the

upstream land surface within the footprint of the flux measurement as the offshore distance increases. As a result of the influence of the upstream land surface, the neutral drag coefficient is not correlated with the atmospheric bulk Richardson number within the first 5 km off the coast. For offshore distances larger than 5 km the correlation between the neutral drag coefficient and the atmospheric bulk Richardson number agrees with the correlation for onshore flow, and the correlation between the friction velocity and the mean square slope of the short waves is also consistent with that for onshore flow.

With offshore flow the mean square slope of the short waves generally decreases with offshore distance and the mean square slope of the long waves generally increases with offshore distance. The spatial variation of the mean square slopes of the short and long waves are apparently due to the energy transfer from wind-driven young short waves to long waves through wave-wave interactions. With onshore flow the spatial variation of the mean square slope of both short and long waves is similar to the offshore flow case, except within 2 km offshore, the mean square slope of the long waves seems to increase slightly toward the coastline apparently due to shoaling.

The dependence of the neutral drag coefficient on the bulk Richardson number probably results from a relationship between the surface roughness and stability and the influence of advection of turbulence from the upstream land surface. This study demonstrates the complexity of air-sea interaction in the coastal zone, and the importance of simultaneous observations of atmospheric conditions and sea state. With the influence of the turbulence from the land surface, the measured momentum flux does not completely reflect the air-sea interaction. The wave age calculated using the observed momentum flux may not represent the true influence of wave state. The interaction between the momentum flux and the variation of the surface waves for the offshore case needs to be further studied with detailed wave spectra.

Acknowledgments. The comments of Bill Plant, Sean Burns, and two anonymous reviewers are greatly appreciated. We gratefully acknowledge Edward Dumas for collecting and processing the LongEZ aircraft data. The waverider buoy data were collected by T.H.C. Herbers with funding from the Office of Naval Research Coastal Dynamics Program. We are also thankful to the support from the Field Research Facility of the US Army Corps of Engineers at Duck, North Carolina. This work is supported by the Office of Naval Research. Jielun Sun is supported by grant N00014-97-1-0245, Douglas Vandemark is supported by grant N0001497F0179, Larry Mahrt and Dean Vickers are supported by grant N00014-97-1-0279, and Timothy Crawford and Christoph Vogel are supported by grant N00014-97-F-0123. The National Center for Atmospheric Research is sponsored by the National Science Foundation.

References

Al-Zanaidi, M. A., and W. H. Hui, Turbulent air flow over water waves: A numerical study, *J. Fluid Mech., 148*, 225-246, 1984.

Anctil, F., M. A. Donelan, Air-water momentum flux observations over shoaling waves, *J. Phys. Oceanogr., 26*, 1344-1353, 1996.

Barrick, D. E., Wind dependence of quasi-specular microwave sea scatter, *IEEE Trans. Antennas Propag., 22*, 135-136, 1974.

Brown, G. S., Estimation of surface wind speeds using satellite-borne radar measurements at normal incidence, *J. Geophys. Res., 84*, 3974-3978, 1979.

Brown, G. S., H. R. Stanley, and N. A. Roy, The wind-speed measurement capability of spaceborne radar altimeters, *IEEE J. Oceanic Eng., 6*, 59-63, 1981.

Cox, C., and W. Munk, Statistics of the sea surface derived from sun glitter, *J. Mar. Res., 13*, 198-227, 1954.

Crawford, T. L., and R. J. Dobosy, A sensitive fast-response probe to measure turbulence and heat flux from any airplane, *Boundary Layer Meteorol., 59*, 257-278, 1992.

Crawford, T. L., R. T. McMillen, T. P. Meyers, and B. B. Hicks, Spatial and temporal variability of heat, water vapor, and carbon dioxide, and momentum air-sea exchange in a coastal environment, *J. Geophys. Res., 98*, 12,869-12,880, 1993.

Crescenti, G. H., T. L. Crawford, and E. J.Dumas, Data report: LongEZ(N3R) participation in the 1999 Shoaling Waves Experiment (SHOWEX) spring pilot study, *NOAA Tech. Memo. ERL ARL-232*, Natl. Oceanic and Atmos. Admin., Washington, D. C., 1999.

Donelan, M. A., The dependence of the aerodynamic drag coefficient on wave parameters, In *First International Conference on Meteorological and Air/Sea Interaction of the coastal Zone*, pp. 381-387, Am. Meteorol. Soc., Boston, Mass., 1982.

Donelan, M. A., Air-sea interaction. in *Ocean Engineering Science*, edited by B. LeMehaute and D. M. Hanes, pp. 239-291, John Wiley, New York, 1990.

Donelan, M. A., F. W. Dobson, S. D. Smith, and R. J. Anderson, On the dependence of sea surface roughness on wave development, *J. Phys. Oceanogr., 23*, 2143-2149, 1993.

Dyer, A. J., A review of flux profile relationships, *Boundary Layer Meteorol., 7*, 363-372, 1974.

Freilich, M. H. R., and R. T. Guza, Nonlinear effects of shoaling surface gravity waves, *Philos. Trans. R. Soc. London, Ser. A, 311*, 1-41, 1984.

Geernaert, G. L., Measurements of the angle between the wind vector and wind stress vector in the surface layer over the North Sea, *J. Geophys. Res., 93*, 8215-8220, 1988a.

Geernaert, G. L., Drag coefficient modeling for the near coastal zone, *Dyn. Atmos. Oceans, 11*, 307-322, 1988b.

Geernaert, G. L., and W. J. Plant, *Surface Waves and Fluxes*, Kluwer Acad., Norwell, Mass., 1990.

Geernaert, G. L., K. B. Katsaros, and K. Richter, Variation of the drag coefficient and its dependence on sea state, *J. Geophys. Res., 91*, 7667-7679, 1986.

Geernaert, G. L., S. E. Larsen, and F. Hansen, Measurements of the wind stress, heat flux, and turbulence intensity during storm conditions over the North Sea, *J. Geophys. Res., 92*, 13,127-13,139, 1987.

Geernaert, G. L., F. Hansen, M. Courtney, and T. Herbers, Directional attributes of the ocean surface wind stress vector, *J. Geophys. Res., 98*, 16,571-16,582, 1993.

Hasselmann, K., et al., Measurements of wind-wave growth and swell decay during the Joint North Sea Wave Project (JONSWAP), *Dtsch. Hydrogr. Z., Suppl., Ser A 8(12)*, 1973.

Horst, T. W., and J. C. Weil, How far is far enough?: The fetch requirements for micrometeorological measurement of surface fluxes, *J. Atmos. Oceanic Technol., 11*, 1018-1025, 1994.

Hwang, P. A., and O. H. Shemdin, The dependence of sea surface slope on atmospheric stability and swell conditions, *J. Geophys. Res., 93*, 13,903-13,912, 1988.

Keller, W. C., W. J. Plant, and D. E. Weissman, The dependence of the X band microwave sea return on atmospheric stability and sea state, *J. Geophys. Res., 90*, 1019-1029, 1985.

Kitaigorodskii, S. A., *The Physics of Air-Sea Interaction*, translated from Russian, 273 pp., Isr. Program for Sci. Transl., Jerusalem, 1973.

Kraus, E. B., and J. A. Businger, *Atmosphere-Ocean Interaction*, Oxford Univ. Press, New York, 1994.

Mahrt, L., The coastal zone, in *Air-Sea Exchange: Physics, Chemistry, and Dynamics*, edited by G. L. Geernaert, Kluwer Acad., Norwell, Mass., 1999.

Mahrt, L., D. Vickers, J. Howell, J. Højstrup, J. M. Wilczak, J. Edson, and J. Hare, Sea surface drag coefficient in the Risø Air Sea Experiment, *J. Geophys. Res., 101*, 14,327-14,335, 1996.

Mahrt, L., D. Vickers, J. Edson, J. Sun, J. Højstrup, J. Hare, and J.M. Wilczak, Heat flux in the coastal zone. *Boundary Layer Meteorol., 86*, 421-446, 1998.

Nordeng, T. E., On the wave age dependent drag coefficient and roughness length at sea, *J. Geophys. Res., 96*, 7167-7174, 1991.

Paulson, C. A., The mathematical representation of wind speed and temperature profiles in the unstable atmospheric surface layer, *J. Appl. Meteorol., 9*, 857-861, 1970.

Plant, W. J., W. C. Keller, V. Hesany, K. Hays, K. W. Hoppel, and T. V. Blanc, Measurements of the marine boundary layer from an airship, *J. Atmos. Oceanic Technol., 15*, 1433-1458, 1998.

Rieder, K. F., J. A. Smith, and R. A. Weller, Observed directional characteristics of the wind, wind stress, and surface waves on the open ocean, *J. Geophys. Res., 99*, 22,589-22,596, 1994.

Smedman, Ann-Sofi, H. Bergström, and U. Högström, Spectra, variances and length scales in a marine stable boundary layer dominated by a low level jet, *Boundary Layer Meteorol., 76*, 211-232, 1995.

Smith, S. D., Wind stress and heat flux over the ocean in gale force winds, *J. Phys. Oceanogr., 10*, 709-726, 1980.

Sun, J., Diurnal variations of thermal roughness height over a grassland, *Boundary Layer Meteorol., 92*, 407-427, 1999.

Torrence, C., and G. P. Compo, A practical guide to wavelet analysis, *Bull. Am. Meteorol. Soc., 79*, 61-78, 1998.

Vandemark, D., J. B. Edson, and B. Chapron, Altimeter estimation of sea surface wind stress for light to moderate winds, *J. Atmos. Oceanic Technol., 14*, 716-722, 1997.

Vandemark, D., T. Crawford, R. Dobosy, T. Elfouhaily, and B. Chapron, Sea surface slope statistics from a low-altitude aircraft, *IEEE Proc. of IGARSS, Hamburg, 1999.*

Vandemark, D., P. D. Mourad, T. L. Crawford, C. A. Vogel, J. Sun, S. A. Bailey, and B. Chapron, Measured changes in ocean surface roughness due to atmospheric boundary layer rolls, *J. Geophys. Res., 106*, 4639-4654, 2001.

Vickers, D., and L. Mahrt, Fetch limited drag coefficients, *Boundary Layer Meteorol., 85*, 53-79, 1997a.

Vickers, D., and L. Mahrt, Quality control and flux sampling problems for tower and aircraft data, *J. Atmos. Oceanic Technol., 14*, 512-526, 1997b.

Vickers, D., and L. Mahrt, Observations of non-dimensional wind shear in the coastal zone, *Q. J. R. Meteorol. Soc., 125*, 2685-2702, 1999.

Vickers, D., and L. Mahrt, J. Sun, and T. Crawford, Structure of off-shore flow, *Mon. Weather Rev.*, in press, 2001.

Weller, R. A., M. A. Donelan, M. G. Briscoe, and N. E. Huang, Riding the crest: A tale of two wave experiments, *Bull. Am. Meteorol. Soc., 14*, 835-848, 1991.

Wu, J., Sea-surface slope and equilibrium wind-wave spectra, *Phys. Fluids, 15*, 741-747, 1972.

Wu, J., Effects of atmospheric stability on ocean ripples: A comparison between optical and microwave measurements, *J. Geophys. Res., 96*, 7265-7269, 1991.

T. Crawford, NOAA/FRD, 1750 Foote Drive, Idaho Falls, ID 83402. (tim.crawford@noaa.gov)

L. Mahrt and D. Vickers, College of Oceanic and Atmospheric Sciences, Oregon State University, Corvallis, OR 97331. (mahrt@oce.orst.edu; vickers@oce.orst.edu)

J. Sun, National Center for Atmospheric Research, P.O. Box 3000, Boulder, CO 80307-3000. (jsun@ucar.edu)

D. Vandemark, NASA/GSFC, Code 972, Wallops Island, VA 23337. (vandemark@gsfc.nasa.gov)

C. Vogel, NOAA/ATDD, P.O. Box 2456, Oak Ridge, TN 37831-2456. (vogel@atdd.noaa.gov)

(Received March 2, 2000; revised September 27, 2000; accepted October 5, 2000.)